THE MAGNETIC SUSCEPTIBILITY OF SOME THIOUREA-COORDINATED TRANSITION METAL HALIDES IN THE PARA-MAGNETIC AND ANTIFERRO-MAGNETIC STATES

Thesis for the Degree of Ph. D.

MICHIGAN STATE UNIVERSITY

Howard Jay Van Till

1965

This is to certify that the

thesis entitled

THE MAGNETIC SUSCEPTIBILITY OF SOME THIOUREA-COORDINATED TRANSITION METAL HALIDES IN THE PARA-MAGNETIC AND ANTIFERRO-MAGNETIC STATES

presented by

Howard Jay Van Till

has been accepted towards fulfillment
of the requirements for

Ph. D. degree in Physics

Robert D. Spence
Major professor

Date July 23, 1965

ABSTRACT

THE MAGNETIC SUSCEPTIBILITY OF SOME THIOUREA-COORDINATED TRANSITION METAL HALIDES IN THE PARA-MAGNETIC AND ANTIFERRO-MAGNETIC STATES

by Howard Jay Van Till

Magnetic susceptibility measurements were made on single crystal and powdered samples of thiourea-coordinated transition metal halides having the chemical formulas $CoCl_2 \cdot 4[(NH_2)_2CS]$, $MnCl_2 \cdot 4[(NH_2)_2CS]$, and $NiBr_2 \cdot 6[(NH_2)_2CS]$. Each of these materials was observed to undergo a transition from the paramagnetic to the antiferromagnetic state at low temperatures. On the basis of the behaviour of the magnetic susceptibility an attempt has been made to identify the directions of the sublattice magnetizations, and a comparison of the measured values of the parallel susceptibility has been made with the results of recent calculations based on the Ising model.

The magnetic susceptibility of all samples was measured by the ac mutual inductance method using a commercial mutual inductance bridge operating at 17 cps. The temperature of the sample was determined by measuring the vapor pressure of the He^3 or He^4 bath in which the sample was immersed.

The results of the measurements on $Co(tu)_4Cl_2$ indicate that it has an antiferromagnetic transition at 0.93°K. The sublattice magnetization vectors lie along or near to the c axis of this tetragonal crystal and a simple two-sublattice model is investigated.

The behavior of the magnetic susceptibility of $Mn(tu)_4Cl_2$ shows that this tetragonal crystal has an antiferromagnetic transition temperature of 0.56°K. However, the sublattice magnetization vectors do not lie near the c axis as was the case for $Co(tu)_4Cl_2$. A two-sublattice model in which the magnetization vectors lie in the ab plane is suggested but leads to some difficulties which can only be resolved by measurements at lower temperatures.

The thiourea-coordinated nickel bromide, $Ni(tu)_6Br_2$, exhibits the most unusual behavior of the three materials here reported. The susceptibility data leads to the conclusion that this material has two transitions of the antiferromagnetic type at 2.0°K and 2.2°K respectively. This conclusion is supported by specific heat data which shows peaks in the specific heat at these temperatures. Furthermore, along none of the principal magnetic axes does the susceptibility approach zero at low temperatures. Thus a simple two-sublattice model can be eliminated immediately and a four-sublattice model, with the magnetization vectors lying in the ac plane of this monoclinic crystal, is suggested.

THE MAGNETIC SUSCEPTIBILITY OF SOME THIOUREA-COORDINATED TRANSITION METAL HALIDES IN THE PARA-MAGNETIC AND ANTIFERRO-MAGNETIC STATES

By

Howard Jay Van Till

A THESIS

Submitted to
Michigan State University
in partial fulfillment of the requirements
for the degree of

DOCTOR OF PHILOSOPHY

Department of Physics and Astronomy

1965

DEDICATION

This thesis is dedicated to my wife and parents who have provided the help, encouragement, and patience to make this work possible.

ACKNOWLEDGMENTS

The author wishes to express his sincere appreciation and thanks to Dr. J. A. Cowen and Dr. R. D. Spence for their invaluable aid and encouragement in this work; to Dr. H. Forstat and Dr. T. O. Woodruff for their suggestions during the preparation of this thesis; to Richard and Carolyn Au for their x ray work and assistance in taking data; to Charles Taylor and George Johnston for their computer work; to the electronic and machine shop personnel for their assistance in the construction of the apparatus; and to the National Science Foundation and Army Research Office (Durham) for their support of both the author and this project.

TABLE OF CONTENTS

LIST OF TABLES

LIST OF FIGURES

LIST OF APPENDICES

I. INTRODUCTION

Measurements of the magnetic susceptibilities of metals and alloys of the transition elements first led Néel[1] to introduce the concept of antiferromagnetism. He was able to explain the qualitative features of the experim ental results by postulating that the magnetic moments of the magnetic ions were arranged in an alternating antiparallel pattern. Since that time this concept has been shown to be valid for many metals and insulators and has been the subject of much experimental and theoretical work.

Information concerning the nature of the antiferromagnetic state can be obtained from a variety of experiments, including magnetic susceptibility, neutron diffraction, x ray diffraction, electron spin resonance, nuclear magnetic resonance, specific heat, thermal and electrical conductivity, and others. Each of these measurements contributes to the description of the antiferromagnetic state of a material, and a complete description must include all of these properties.

The work described in this thesis has a three-fold purpose.

1. The construction of a system capable of measuring the magnetic susceptibility of antiferromagnetic materials in the He^3 and He^4 temperature range (0.40°K to 4.2°K).

2. The measurement of the magnetic susceptibility of materials not previously studied or known to be antiferromagnetic with transition temperatures in this temperature range.

3. The discovery of new antiferromagnetic materials suitable for further investigation by methods already existing in this laboratory, such as proton magnetic resonance and specific heat.

The main body of this report consists of a description of the experimental apparatus and procedure, a brief discussion of some of the existing theories of antiferromagnetism, and a presentation and discussion of the behavior of the magnetic susceptibility of three antiferromagnetic materials discovered in this work.

II. EXPERIMENTAL APPARATUS AND PROCEDURE

A. General Method

Magnetic susceptibility was measured by the ac mutual inductance method. This method utilizes the fact that the mutual inductance of two concentric solenoids is proportional to the magnetic permeability of the space or material within the solenoids. If we let ΔM be the difference in the mutual inductance of a set of coils with and without a sample in some specified volume then ΔM will be proportional to the difference in the permeability of that volume and hence proportional to the susceptibility of the sample.

$$\Delta M = C\chi, \tag{2.1}$$

where χ = the susceptibility of the sample.

The proportionality constant C in (2.1) can be evaluated in two ways. (1) A theoretical value can be calculated using the geometry of the system of coils and sample. (2) An experimental value can be obtained by measuring ΔM for a sample with known susceptibility. Method (1) is ideal when the geometry of the system is simple and known to a high degree of accuracy. However, in the experiments reported here method (2) has been used since it relaxes the requirements on coil construction and since standard samples with reasonably well known

susceptibilities are readily available. Standards used here were single crystals of ferric ammonium alum and potassium chrome alum with susceptibilities of $\frac{9.02 \times 10^{-3}}{T}$ cc/gm and $\frac{3.66 \times 10^{-3}}{T}$ cc/gm in their Curie Law regions.[2,3]

B. The Mutual Inductance Coils and Bridge

Figure 1 shows the geometry of the coils and sample. The primary consists of two concentric solenoids which are wound such that the condition

$$\frac{N_1}{N_2} = \left(\frac{D_2}{D_1}\right)^2 \qquad (2.2)$$

is approximately satisfied, where

N_1 = 6450 = number of turns on inner solenoid,

N_2 = 3840 = number of turns on outer solenoid,

D_2 = 3.5 cm = diameter of outer solenoid,

D_1 = 2.6 cm = diameter of inner solenoid.

These two solenoids are connected in series so as to oppose each other. If (2.2) is exactly satisfied, then in the absence of a sample the net magnetic flux through the entire primary is zero. Thus the primary has no magnetic dipole moment and will not interact strongly with nearby magnetic materials. However, the magnetic field intensity at the sample position is not zero and in fact has the value

$$H = C\left(\frac{2\pi}{5}\right)\left(\frac{N_1 - N_2}{L}\right) I \text{ oersteds}, \qquad (2.3)$$

where

I = current through primary (amperes),

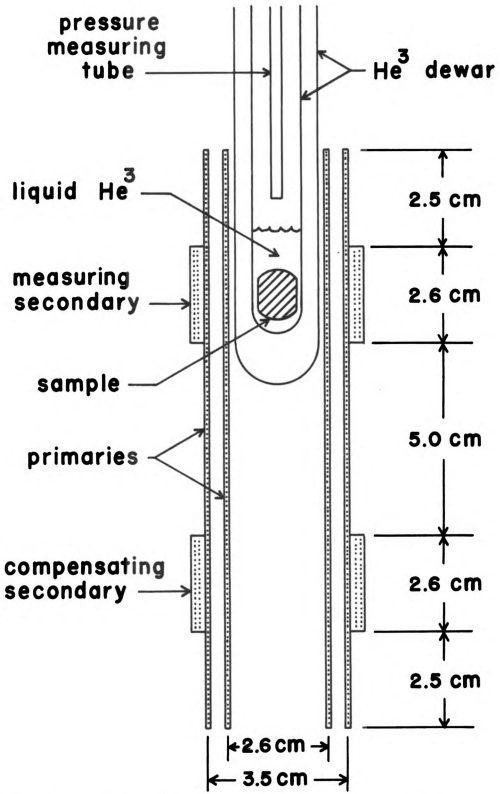

Fig. 1. The geometry of the mutual inductance coils and sample.

L = length of primary (cm),

C = constant, slightly less than one due to the finite length of the solenoids.

Therefore, the presence of a sample with $\chi \neq 0$ will introduce a change in the magnetic flux which can be measured by the secondary. An additional secondary coil identical to the measuring secondary and connected in opposition to it is used to compensate for any flux resulting from the fact that (2.2) may not be exactly satisfied.

The coils were wound with #36 Nylclad coated copper wire. The method of construction is similar to that described by Abel, Anderson and Wheatley.[4]

The mutual inductance was measured with a Cryotronics model 17B electronic mutual inductance bridge[5] operating at 17 cps. When the bridge is balanced the mutual inductance being measured is equal to the product of the course and fine dial readings multiplied by 50×10^{-5} μh. The sensitivity of the coils was such that the difference in dial readings with and without sample had to be multiplied by 2.2×10^{-8} in order to obtain the susceptibility. Thus:

$$\chi \text{ (cc/mole)} = (P_s - P_e)\left(\frac{M.W.}{W_s}\right) \times 2.2 \times 10^{-8}, \qquad (2.4)$$

where

P_s = Product of course and fine dial settings with sample in coils,

P_e = Product of course and fine dial settings without sample in coils (empty),

M.W. = molecular weight of sample,

W_s = actual weight of sample in grams.

The mutual inductance bridge was most easily balanced by applying the primary coil voltage to the x axis of an oscilloscope and the output of the bridge amplifier to the y axis. An offbalance condition appears as an ellipse on the scope, while a perfectly balanced condition appears as a single horizontal line. The resistive balance primarily controls the tilt of the ellipse and the inductive balance primarily controls the openness of the ellipse. Thus it was quite easy to judge what adjustments were necessary to obtain balance.

C. He^3 Dewar and Sample

As shown in Fig. 1 the coils are mounted on the outside of a glass He^3 dewar. This dewar is shown in more detail in Fig. 2. As can be seen, the design is very simple and only very crude attempts were made to minimize radiation heat leaks. However, this system worked very well and temperatures as low as 0.4°K could be reached. For lower temperatures one should provide a more efficient radiation trap and possibly provide larger pumping lines.

The sample, ground in the shape of a short cylinder with rounded ends, was of such a size as to slide freely down the inner tube, yet maintain its orientation with respect to the axis of the coils. It was held in place

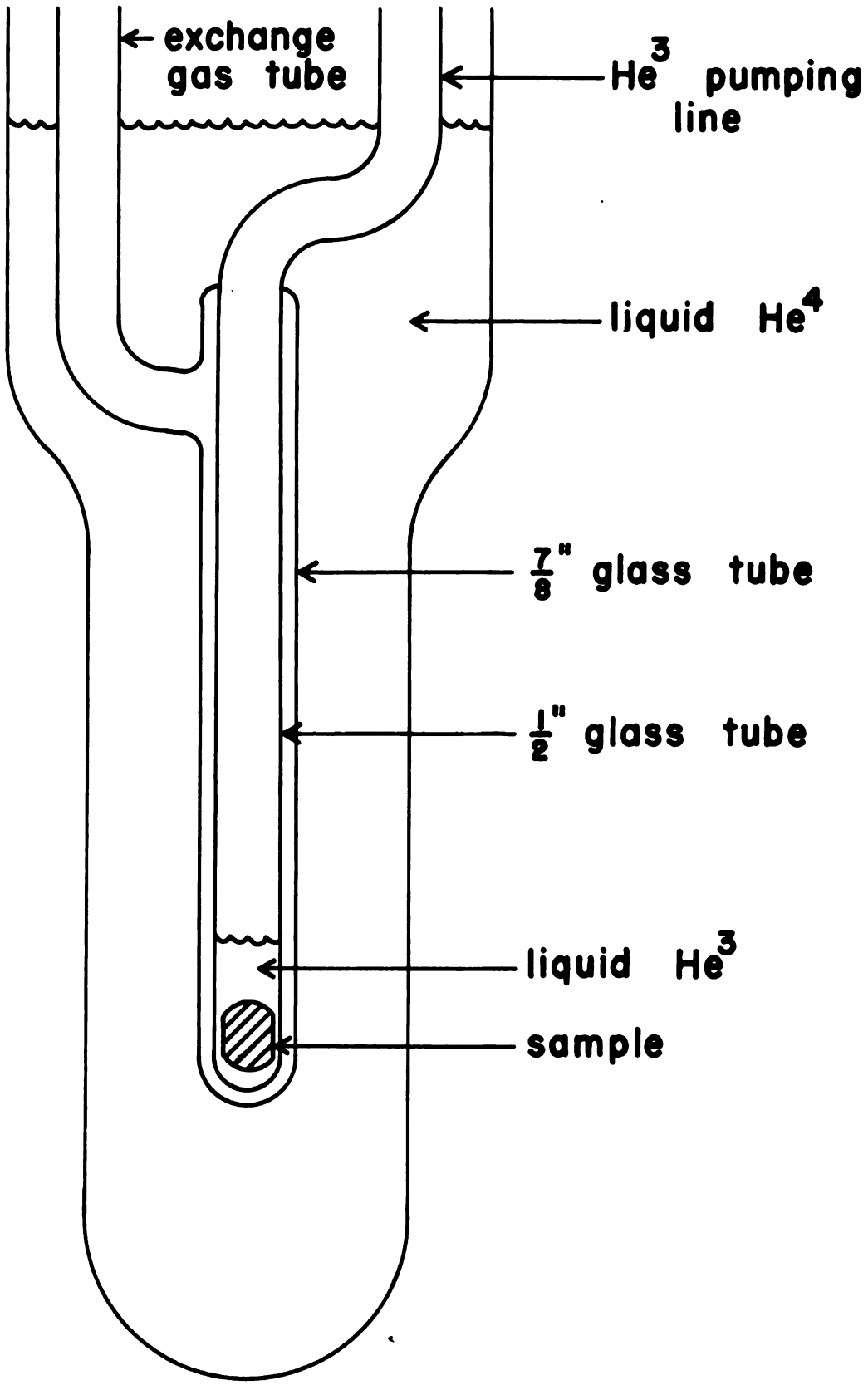

Fig. 2. The He^3 dewar.

at the bottom of the dewar by three or four drops of Dow Corning 704 fluid which freezes upon cooling.

For measurements below 1.1°K the sample was immersed in liquid He^3. The temperature was measured by noting the vapor pressure of the He^3 as sampled by a 1/8" teflon tube which extended from an NRC Alphatron pressure gauge to a point just above the surface of the liquid He^3. The guage was calibrated by measuring the susceptibility of ferric ammonium alum and potassium chrome alum, which are known to obey the Curie law in the He^3 temperature range, as a function of the pressure gauge readings. The value of the susceptibility gives the temperature corresponding to the indicated pressure.

D. Experimental Procedure

Listed below is a typical sequence of operations during a single experimental run

1. Pre-cool to liquid nitrogen temperature and evacuate both sections of the He^3 dewar to a pressure of about 10^{-5} mm. Hg.

2. Take a reading of the mutual inductance, making sure that thermal equilibrium has been reached.

3. Isolate the inner and outer chambers of the He^3 dewar; introduce He^4 gas into the exchange gas section at a pressure of about 200 μ and He^3 gas into the He^3 section at a pressure of about 1 mm.

4. Transfer liquid He^4 into the large He^4 dewar and immediately begin to pump on the He^4.

5. While pumping on the He^4, introduce the remainder of the He^3 gas into the He^3 dewar and allow the He^3 to liquify.

6. Allow the system to come to thermal equilibrium at the lowest He^4 bath temperature ($\sim$ 1.1°K).

7. Remove exchange gas from He^3 dewar.

8. By pumping on the He^3, lower the temperature of the He^3 bath and crystal in a stepwise manner, maintaining each different pressure until M ceases to change. Thermal equilibrium was attained much more quickly when decreasing the temperature than when allowing the temperature to drift up.

9. When finished with measurements below 1.1°K admit some exchange gas again ($\sim$ 100 μ) and pump out the remaining He^3.

10. Allow the He^4 bath to warm up to 4.2°K.

11. Decrease the He^4 bath temperature and again measure M at appropriate temperature intervals down to 1.1°K.

E. Data Reduction and Experimental Accuracy

The experimental procedure above describes how M(T) was measured. But what we really want to know is $\Delta M(T)$. Theoretically one should be able to simply take the difference of M(T) measured with and without a sample.

But in actual practice it was found that an additional constant had to be included in this difference in order to account for small changes in the coil characteristics from run to run.

Therefore

$$\Delta M(T) = M(T)_{\text{with sample}} - M(T)_{\text{without sample}} + Mo \ , \quad (2.5)$$

where

$$Mo = \lim_{\frac{1}{T} \to 0} \left[M\left(\frac{1}{T}\right)_{\text{without sample}} - M\left(\frac{1}{T}\right)_{\text{with sample}} \right] . \quad (2.6)$$

This method does have the disadvantage, however, of placing too much emphasis on the measurements of M at liquid nitrogen temperature. If thermal equilibrium has not been attained a constant error will be introduced. An alternative method is to construct the system such that the sample can be physically moved in and out of the coils. This was not done in the He^3 cryostat but for many of the measurements in the He^4 temperature range the He^3 dewar was removed and replaced by a sample holder which could be easily moved in and out of the coil region. This method was very helpful in checking earlier data, and in the case of $Ni(tu)_6Br_2$, where the susceptibility is small, it proved to be the only reliable method. The overall accuracy of the data presented in this report is estimated at $\pm$ 10%.

Strictly speaking, the experimental values of the susceptibility should be corrected according to the relation

$$\chi = \frac{\chi_{exp}}{[1 + (4\pi/3 - N)\,\chi_v]}, \qquad (2.7)$$

where N is the demagnetization factor along the axis of measurement and χ_v is the volume susceptibility. Since this correction would amount to 1% or less for this work it was ignored.

F. Sample Preparation and Chemical Analysis

All samples used in this study were grown from aqueous solutions of the transition metal halide and thiourea. Although good, large single crystals of these materials were not difficult to obtain, a brief description of the procedure is given here.

Large, dark-blue, bipyramidal crystals of $Co(tu)_4Cl_2$ were easily grown at room temperature by slow evaporation of an aqueous solution containing $CoCl_2 \cdot 6H_2O$ and $(NH_2)_2CS$ in the ratio of approximately 2:1 by weight. The exact composition of the solution was not very critical and good samples could be grown with a wide range of constituent ratios.

Large, dark yellow-green, prismatic crystals of $Ni(tu)_6Br_2$ were readily grown at room temperature by slow evaporation of an aqueous solution of $NiBr_2$ and $(NH_2)_2CS$ in the ratio of approximately 1:1 by weight. It was found, however, that thiourea tends to act as a reducing agent and small amounts of nickel would collect on the sides of the beaker. Therefore the solution was filtered every few days and placed in a clean beaker.

$Mn(tu)_4Cl_2$ required a little more care and patience than needed for the other materials described above. It was found that the weight ratio of $MnCl_2 \cdot 4H_2O$ to $(NH_2)_2CS$ had to be approximately 20:1 at room temperature. Good crystals would grow at room temperature but very slowly. It was found that crystals could be grown faster by preparing a solution with a 5:1 ratio of constituents and allowing the solution to cool slowly from 50°C.

The chemical constitution of our samples was determined by subjecting them to a chemical analysis for their nitrogen, sulfur, and metal content. Below is a list of the theoretical and measured compositions. The agreement between theoretical and measured values is sufficiently close to assure us that we are using the correct chemical formulas.

Table 1.--Results of chemical analysis of samples.

Sample	Per Cent N		Per Cent S		Per Cent Metal	
	theor.	meas.	theor.	meas.	theor.	meas.
$Co(tu)_4Cl_2$	25.8	24.5	29.5	29.3	13.6	12.4
$Mn(tu)_4Cl_2$	26.0	24.5	29.8	28.7	12.8	12.1
$Ni(tu)_6Br_2$	24.9	24.2	28.5	28.4	8.7	8.9

III. BRIEF DISCUSSION OF EXISTING THEORIES

A. The Scope of This Discussion

A complete discussion of all theories pertaining to the behavior of antiferromagnetic materials is both impractical and unnecessary. There exist many comprehensive reviews[6-8] of this subject to which the reader is directed for further discussion and references. As a basis for the discussion of Chapter IV, I shall review here the origin of the spin-dependent interactions, two common approximations to this interaction potential (molecular field approach and Ising model), and the results of series expansion calculations on the magnetic susceptibility of the Ising antiferromagnet.

B. Direct and Indirect Exchange-- Early Theories

In order to account for the ordered state of spin systems it is necessary to know the nature and origin of spin-dependent forces. Why do neighboring spins prefer a parallel or antiparallel arrangement? In the early work of Heisenberg, Dirac, and others, perturbation theory was applied to the atomic orbitals of neighboring ions, each with one or more unpaired spins outside of a nonmagnetic

core. Consider the case of one unpaired electron on each ion. If the orbital wave functions ψ_i and ψ_j of the unpaired (magnetic) electrons on atoms k and j are orthogonal, the perturbation caused by the Coulomb repulsion between these electrons splits the original ground state, which had a two-fold exchange degeneracy, into two states separated in energy by an amount $2J_{ij}$, where

$$J_{ij} = \int dv_1\, dv_2\, \psi_j^*(\vec{r}_1)\, \psi_i^*(\vec{r}_2)\, \frac{e^2}{|\vec{r}_1-\vec{r}_2|}\, \psi_j(\vec{r}_1)\, \psi_i(\vec{r}_2), \quad (3.1)$$

and $\vec{r}_1$ and $\vec{r}_2$ are the position vectors of electrons 1 and 2 in this two-electron formulation of the problem. J_{ij} is positive so that the upper state is one with a symmetric orbital function and an antisymmetric ($S_{tot} = 0$, spins antiparallel) spin function, while the ground state has an antisymmetric orbital function and a symmetric ($S_{tot} = 1$, spins parallel) spin function. This splitting is caused by the Coulomb interaction between orbitals and the restrictions of the Pauli exclusion principle. Although the splitting is orbital in origin the energy can be expressed formally in terms of the relative orientation of the spins. Let $\langle V_{ij}^{sp} \rangle$ be the expectation value of the spin-dependent part of the electron-electron interaction. The proper energy levels can be obtained by letting

$$\langle V_{ij}^{sp} \rangle = -\tfrac{1}{2} J_{ij} \left(1+4 \langle \vec{S}_i \cdot \vec{S}_j \rangle\right) . \quad (3.2)$$

Noting that $\langle \vec{S}_i \cdot \vec{S}_j \rangle = \frac{1}{2}(\langle S_{tot}^2 \rangle - \langle S_i^2 \rangle - \langle S_j^2 \rangle)$, it can be seen that results of the perturbation calculation are retained.

Generalizing the problem to a macroscopic crystal instead of an isolated pair of atoms, the spin-dependent part of the electron-electron interaction has been written as

$$V^{sp} = \sum_{ij} -\tfrac{1}{2}J_{ij}(1+4\vec{S}_i \cdot \vec{S}_j) , \qquad (3.3)$$

where the summation is to be carried over all pairs of atoms in the crystal. This form is often called the Heisenberg interaction.

One problem with this formulation is that J_{ij} is always positive (ferromagnetic) and cannot account for an antiferromagnetic interaction. This can in some cases be overcome by using nonorthogonal orbitals in which case $\frac{e^2}{r_{12}}$ is replaced by the total Hamiltonian in the expression for J_{ij}. If the electrons are in an attractive potential, J_{ij} may become negative. In either case discussed above the effect depends on the direct contact or overlap of wave functions and has traditionally been called direct exchange.

Most antiferromagnetic materials are insulators in which the magnetic ions are separated by non-magnetic ions or groups of ions. Early thinking on this matter led to the idea that direct exchange played an unimportant role in interactions between magnetic ions in such cases and a different effect was sought

By virtue of the fact that this interaction acts over large distances it was given the name superexchange (or indirect exchange). Without going into the mathematical details, which may be found elsewhere[6,9,10], let us describe qualitatively the origin of this phenomenon. Consider a three-ion system such as Mn_2O^{++}. The zero-order ground state can be described as

$$Mn^{++} \qquad O^{--} \qquad Mn^{++}$$
$$d_1 \qquad p \qquad d_2$$

where we have concentrated our attention on one of the d electrons in each Mn atom and on two p electrons of the O atom. One possible excited state can be described by

$$Mn^{+} \qquad O^{-} \qquad Mn^{++}$$
$$d_1 d_1' \qquad p \qquad d_2$$

where one of the p electrons from the O atom has gone over to one of the Mn atoms. If one now carries out a perturbation calculation and considers the contributions of the excited states to the true ground state one finds some interesting results. The first-order correction to the energy is zero. The second order correction is independent of the spins of d_1 and d_2. The third order correction to the energy can be written in the form $J \langle \vec{S}_1 \cdot \vec{S}_2 \rangle$.

Thus, once again we have an interaction which can formally be written as in (3.3). In this case, however, the interaction is transmitted by an intermediate non-magnetic ion such as O, S, F, Cl, Br, or I.

C. Exchange Interactions--Modern Theory

The early theories discussed above seemed to have many good qualities but ran into difficulty on many points. The perturbation calculation used in the superexchange problem converges quite slowly and has many large non-magnetic terms. Other excitations such as double electron transfer lead to similar results, suggesting that the real mechanism is simpler than assumed. Finally, one does not really know the proper wave functions to use in calculating J_{ij}.

The modern theory of exchange interactions[11], now in its early stages, attempts to treat the problem in a more realistic way. The program consists of two parts:

1. In order to assure a more rapidly converging perturbation series, calculate by means of modern ligand field theory the wave functions of the magnetic and non-magnetic ions in the crystal, neglecting all exchange effects.

2. Using the results of part (1) include now the exchange effects and calculate the interaction characteristics of the magnetic ions.

This program has the advantage that the perturbations are weaker and more rapidly converging. In addition, all interactions are now directly between magnetic ions, the intermediate non-magnetic ions being taken care of by the ligand field calculations. Thus the early distinction between direct and indirect exchange is broken down and new meaning is given to these terms.

Direct exchange now refers only to the effect provided by the electrostatic Coulomb repulsion of electrons. This applies to any pair of magnetic ions regardless of the presence of non-magnetic ions. Such an interaction is always ferromagnetic.

Superexchange is now the second-order effect of a virtual transfer of electrons between magnetic ions. It is a kinetic energy effect related to the fact that when two neighboring spins are parallel their orbital functions are orthogonal, while for antiparallel neighboring spins the spin functions are orthogonal so that their orbital functions may overlap. Such an interaction is always antiferromagnetic and the splitting between parallel and antiparallel states is of the order $\frac{2b^2}{U}$, where U is the Coulomb energy gained by an electron in going from one magnetic ion to another, both of which originally contained the proper number of electrons, and b is the "transfer integral" connecting these states. This new superexchange mechanism depends on a direct contact between wave functions of neighboring magnetic electrons as opposed to the early theory in which the intermediate non-magnetic ion provided the connecting link.

These two effects, direct exchange related to the Coulomb repulsion of electrons, and superexchange related to electron transfer, are the major contributors to

spin-dependent forces in the modern theory of exchange in insulators. In each case the interaction potential can be put in the form (3.3).

D. Approximations to Interaction Potential

1. Preliminary Remarks

From the previous discussion we are led to solve the problem of a system of magnetic ions with an interaction potential of the form

$$V^{sp} = \sum_{i,j} -\tfrac{1}{2}J_{ij}\,(1 + 4\vec{S}_i \cdot \vec{S}_j)\,, \qquad (3.3)$$

where the summation is over all pairs of magnetic ions. This has proved to be an extremely difficult problem and many approximations to (3.3) have been made.

A first simplification can be made by ignoring all but nearest neighbor pairs in the summation of (3.3). In many cases this is a good approximation, but by itself does not lend much simplification to the problem. Thus we are forced to go to a greater degree of approximation. In the following sections I shall describe the principal features of two such approximations.

2. The Molecular Field Approach

The Weiss molecular field approach to antiferromagnetic materials proposed by Néel in 1932 has been responsible for a considerable advance in the qualitative understanding of many properties of antiferromagnetic systems. Let us assume

that we can divide the lattice of magnetic ions into two interpenetrating sublattices A and B. We conceive of the ground state of the system to be one in which all the spins on sublattice A are parallel to each other and anti-parallel to the spins on sublattice B, each sublattice having the same number of spins so that the net magnetic moment is zero. Consider one ion i on one of these sublattices, say A. To simplify the summation in (3.3) let us assume that this ion interacts with z neighbors on sublattice B with an exchange constant J_1, and z' neighbors on sublattice A with exchange constant J_2. Now we can express the interaction potential of atom i on sublattice A as

$$V_i^A = -2J_1\vec{S}_i \cdot \sum_j^z \vec{S}_j - 2J_2\vec{S}_i \cdot \sum_k^{z'} \vec{S}_k \,, \tag{3.4}$$

where the first summation is over the z neighbors on sublattice B and the second summation is over the z' neighbors on sublattice A. Equations (3.4) and (3.3) can be related by

$$V^{sp} = \text{constant} + \sum_i V_i^A + \sum_j V_j^B \,. \tag{3.5}$$

The next approximation consists in replacing the summations in (3.4) by $\overline{z\vec{S}_B}$ and $\overline{z'\vec{S}_A}$ respectively, where $\overline{\vec{S}_A}$ and $\overline{\vec{S}_B}$ are to be considered as statistical averages of the spin on each sublattice. Doing this, (3.4) becomes

$$V_i^A = -2zJ_1\vec{S}_i \cdot \overline{\vec{S}_B} - 2z'J_2\vec{S}_i \cdot \overline{\vec{S}_A} \,. \tag{3.6}$$

Remembering the relation between magnetic moment and spin for an electron,

$$\vec{\mu} = -g\beta\vec{S} \ ,$$

where

g = the spectroscopic splitting factor,

β = the Bohr magneton,

we can write

$$V_i^A = -\frac{2zJ_1}{g^2\beta^2}\ \vec{\mu}_i \cdot \overline{\vec{\mu}_B} - \frac{2z'J_2}{g^2\beta^2}\ \vec{\mu}_i \cdot \overline{\vec{\mu}_A} \ . \qquad (3.7)$$

Now define

$$\vec{H}_{eff}^{A} = \frac{2zJ_1}{g^2\beta^2}\ \overline{\vec{\mu}_B} + \frac{2z'J_2}{g^2\beta^2}\ \overline{\vec{\mu}_A} \ , \qquad (3.8)$$

so that we can write V_i^A in the form

$$V_i^A = -\vec{\mu}_i \cdot \vec{H}_{eff}^{A} \ , \qquad (3.9)$$

with a similar expression for V_j^B, the interaction potential for atom j on sublattice B.

Thus we have now defined an effective magnetic field $\vec{H}_{eff}^{A,B}$ which acts on the magnetic moment of each ion. This is called the molecular or exchange field. It must be emphasized that this is not a real magnetic field but merely a convenient way to express the energy of a magnetic ion coupled to its neighbors by the exchange effect.

With the interactions considered thus far the spin system may assume an antiparallel arrangement but has no preferred directions with respect to crystallographic axes.

This preferred direction can be introduced phenomenologically in the form of an "anisotropy energy" which is a function of the direction of the sublattice magnetization with respect to the crystallographic axes. Good discussions of this subject can be found in references 6 and 12.

Now let us calculate the magnetic susceptibility in the molecular field approximation which we have introduced. For the purposes of this discussion let us write $\vec{H}_{eff}$ in a slightly different form. Note that

$$\vec{M}_{A,B} = 1/2\ N\ \bar{\vec{\mu}}_{A,B} \quad ,$$

where

$\vec{M}_{A,B}$ = the magnetization of sublattice A or B,

N = the total number of magnetic ions per unit volume.

Then we can write

$$\left.\begin{aligned} \vec{H}^{A}_{eff} &= -\alpha\vec{M}_B - \gamma\vec{M}_A \quad , \\ \vec{H}^{B}_{eff} &= -\alpha\vec{M}_A - \gamma\vec{M}_B \quad , \end{aligned}\right\} \quad (3.10)$$

where

$$\left.\begin{aligned} \alpha &= -\frac{2}{N}\left(\frac{2zJ_1}{g^2\beta^2}\right), \\ \gamma &= -\frac{2}{N}\left(\frac{2z'J_2}{g^2\beta^2}\right) \end{aligned}\right\} \quad (3.11)$$

From the theory of paramagnetic susceptibility[13] we know that for a spin only paramagnet (J = S)

$$M = Ng\beta SB_s(y) \quad , \tag{3.12}$$

where $B_s(y)$ is the Brillouin function,

$$B_s(y) = \frac{2S+1}{2S} \coth\left(\frac{2S+1}{2S}y\right) - \frac{1}{2S}\coth\left(\frac{y}{2S}\right), \tag{3.13}$$

$$y = g\beta SH/kT \quad ,$$

H = applied magnetic field

For an antiferromagnet let us calculate M_A or M_B by replacing H with $\left|\vec{H} + \vec{H}_{eff}\right|$ (where $\vec{H}$ and $\vec{H}_{eff}$ are assumed to be parallel). Consider first the case $\vec{H} = 0$. Then

$$M_A = \tfrac{1}{2}Ng\beta SB_s\left(\frac{\left|\alpha\vec{M}_B + \gamma\vec{M}_A\right| Mg\beta S}{kT}\right) \tag{3.14}$$

In the absence of an applied field $\vec{M}_A = -\vec{M}_B$ and $\left|\vec{M}_A\right| = \left|\vec{M}_B\right| = M$, where

$$M = \tfrac{1}{2}Ng\beta SB_s\left(\frac{|\alpha-\gamma|\, Mg\beta S}{kT}\right) . \tag{3.15}$$

M is a decreasing function of temperature and vanishes for $T > T_N$, where T_N can be evaluated in the following manner. We assume that $y = \frac{|\alpha-\gamma|Mg\beta S}{kT}$ is small and replace $SB_s(y)$ by the leading term in the series expansion, $1/3\,(S+1)y$. Thus, for M small we have

$$M = \tfrac{1}{2}Ng\beta \cdot 1/3\,(S+1)\,|\alpha-\gamma|\, MSg\beta/kT \quad . \tag{3.16}$$

This yields for the temperature at which the expansion is most valid

$$T_N = \frac{Ng^2\beta^2S(S+1)}{3k}\,\frac{|\alpha-\gamma|}{2} \quad , \tag{3.17}$$

or

$$T_N = \frac{C}{2}\,|\alpha-\gamma| \quad , \tag{3.18}$$

where C is the Curie constant

$$C = \frac{Ng^2 \beta^2 S(S+1)}{3k} \quad .$$

Next consider the case $T > T_N$ and $H \neq 0$. Again y_A and y_B will be small and $M_{A,B}$ can be approximated by

$$M_A = \tfrac{1}{2}Ng\beta 1/3\ (S+1)\ (H - \alpha M_B - \gamma M_A)\ Sg\beta/kT \quad ,$$

$$\left.\begin{aligned} M_A &= \frac{C}{2T}\ (H - \alpha M_B - \gamma M_A) \quad , \\ M_B &= \frac{C}{2T}\ (H - \alpha M_A - \gamma M_B) \quad . \end{aligned}\right\} \qquad (3.19)$$

But $$\chi H = M_A + M_B \quad . \qquad (3.20)$$

Putting (3.19) into (3.20) we have

$$\chi H = \frac{C}{2T}\ \{2H - (M_A + M_B)\ (\alpha + \gamma)\} \quad , \qquad (3.21)$$

so that

$$\chi = \frac{C}{T+\theta} \quad , \qquad (3.22)$$

where

$$\theta = \frac{C}{2}\ (\alpha + \gamma) \qquad (3.23)$$

For $T < T_N$ we consider two cases.

a. $\vec{H}$ parallel to the sublattice magnetization.

To calculate $\chi_{\parallel}$ we must expand the Brillouin function in powers of H and solve for

$$\chi_{\parallel} = \left| \frac{\vec{M}_A + \vec{M}_B}{H} \right| \quad .$$

The mathematical details are not particularly illuminating and we give here only the general features. $\chi_{\parallel}$ vanishes at $T = 0$ and rises to $\frac{C}{T_N + \theta}$ at $T = T_N$.

b. H perpendicular to the sublattice magnetization.

From Fig. 3 we can see that $\chi_{\perp}H = (M_A + M_B) \sin \phi = 2M \sin \phi$. To obtain $\sin \phi$ as a function of H we note that at the equilibrium value of ϕ the torque on each sublattice must vanish, or

$$| \vec{M}_A \times (\vec{H} + \vec{H}^A_{eff}) | = 0 \quad . \tag{3.24}$$

This leads to

$$2M \sin \phi = \frac{H}{\alpha} \quad , \tag{3.25}$$

so that

$$\chi_{\perp} = \frac{1}{\alpha} = \text{constant} \tag{3.26}$$

Figure 4 summarizes the results of these susceptibility calculations.

The principal feature of the molecular field approximation lies in equation (3.6) where the summation over neighbors is replaced by a statistical average over the whole sublattice. This in effect removes the concept of local interactions and considers each ion to be interacting equally with each member of a given sublattice. Although the constants α and γ defined by (3.11) still contain the factors z and z', these factors only occur in products such as zJ_1 and $z'J_2$ and hence merely allow us to characterize the strength of the interaction by a two-particle parameter J. The result of this averaging over the sublattice as done in (3.6) is that all effects of short range order disappear.

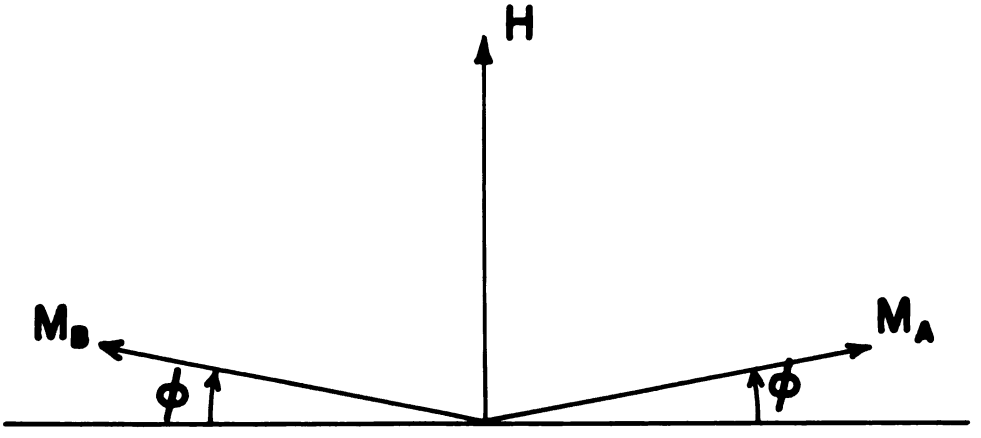

Fig. 3. The effect of a perpendicular magnetic field on the sublattice magnetization vectors.

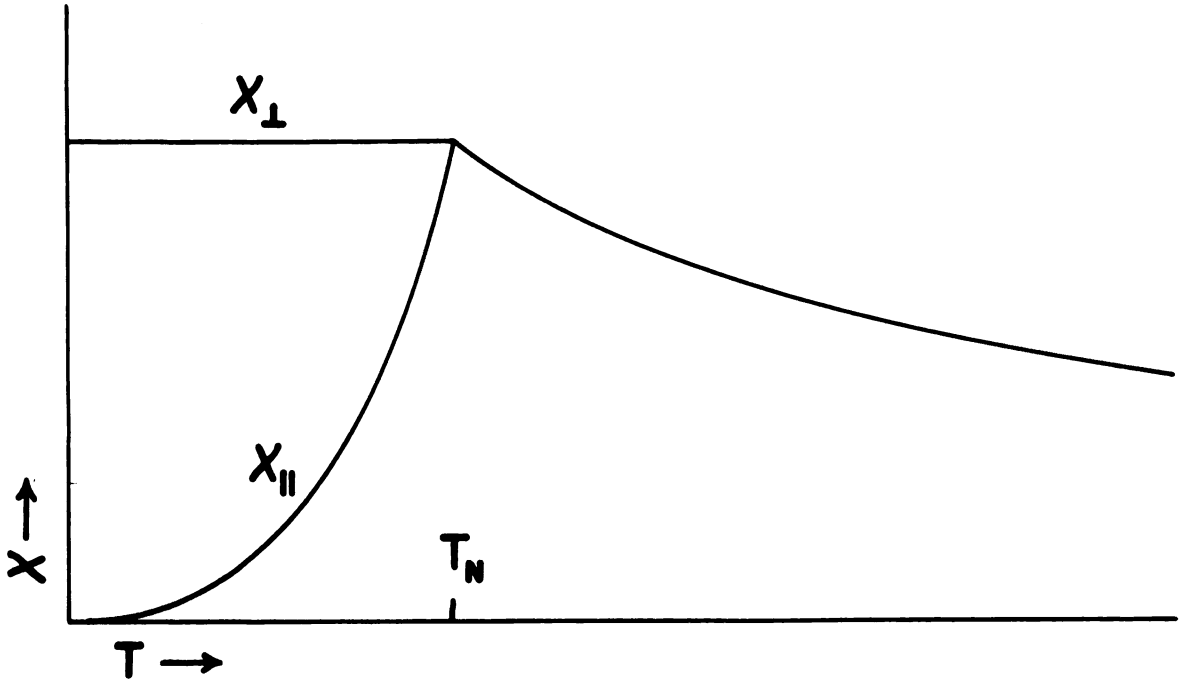

Fig. 4. Sketch of χ vs T in the molecular field approximation.

Only long range ordering is considered. At high temperatures short range ordering is thermally reduced and may certainly be neglected. Some long range ordering is introduced by the application of a magnetic field. Thus in the high temperature limit the molecular field approximation should be quite reasonable. However, near or below T_N short range correlations could surely be expected to influence such properties as the magnetic susceptibility and one must not put too much faith in the details of results obtained above. This has been demonstrated repeatedly by experiment where in general the results agree with the molecular field theory with respect to qualitative features but disagree with respect to quantitative details, except possibly in the high temperature limit.

3. The Ising Model

The Ising model of the exchange interaction simply replaces $\vec{S}_i \cdot \vec{S}_j$ by $S_{zi} S_{zj}$, thus allowing the state of the system to be described by assigning a value of S_z to each magnetic ion. Equation (3.3) is then replaced by

$$V^{sp} = \sum_{ij} -AJ_{ij} S_{zi} S_{zj} \quad , \tag{3.27}$$

where A is a constant which has been given various values by different authors. We will use A = 4 so that for spin ½ atoms the values of V^{sp} in (3.27) range from -J to +J as they would in (3.3)

Let us go back to the two electron problem discussed earlier and compare the energy levels resulting from (3.3) and (3.27). Figure 5 shows the energy level scheme for both potentials and for both signs of J. As can be seen, the level scheme is different for the Heisenberg exchange and the Ising model potentials. The Ising model gives rise to two doublets separated by 2 |J| for either sign of J. On the other hand, the Heisenberg model gives rise to singlet and triplet levels separated by 2 |J| and inverts the order of these levels upon a sign change of J.

In spite of these difficulties the Ising model has been very useful in treating magnetic properties as well as other problems in which the state of the system is described by assigning values of a single-particle parameter to each member of the system. In the next section we shall make use of this Ising model in a statistical treatment of the properties, with emphasis on the magnetic susceptibility, of a system of magnetic ions which undergoes an antiferromagnetic transition.

E. Statistical Mechanics of the Ising Model

1. Formulation of the problem

In the statistical treatment of a problem it is very useful to know the partition function of the system under consideration because from this function many thermodynamic

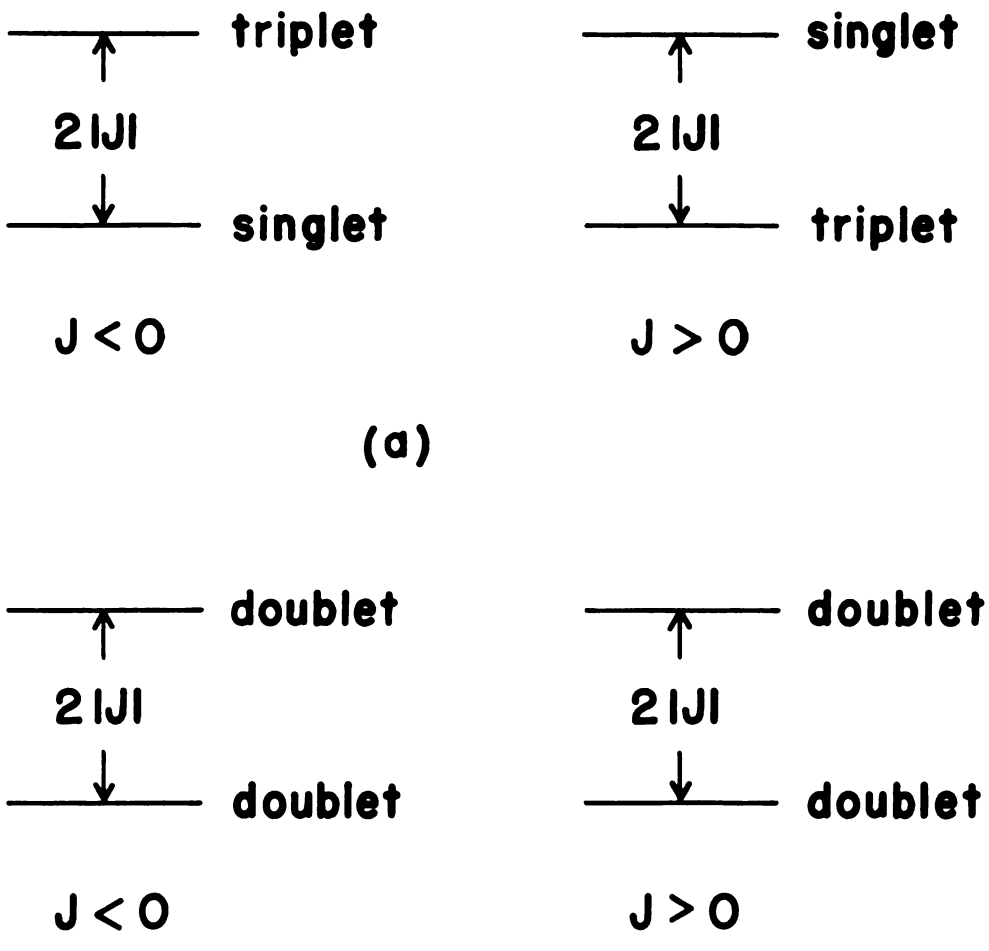

Fig. 5. Energy levels of the two interacting electron problem (a) using the Heisenberg model, (b) using the Ising model.

properties can be calculated. The partition function is defined as

$$Z = \sum_c g_c e^{-E_c/kT} \quad , \tag{3.28}$$

where E_c is an energy state of the system, g_c is the number of states having that energy, and the summation is over all possible energy states. In particular, the magnetic susceptibility of the system is

$$\chi(T) = kT \frac{\partial^2}{\partial H^2} [\ln Z (H,T)] \quad , \tag{3.29}$$

where H is the magnetic field intensity.

Writing down equation (3.28) is very simple but putting in the values of g_c and E_c is often extremely difficult. In our problem E_c is given by

$$E_c = -4J \sum_{i,k} S_{zi}S_{zk} - 2\mu H \sum_i S_{zi} \quad , \tag{3.30}$$

where $\sum_{i,k}$ is a summation over nearest neighbor pairs, $\sum_i$ is a summation over all spins, and $S_z = \pm\frac{1}{2}$. This is obtained from (3.3) by dropping the constant term, considering only nearest neighbor interactions, and adding an energy contribution due to the presence of an applied magnetic field. Now g_c is the number of configurations (sets of S_{zi}) which have the same energy E_c.

2. Low Temperature Expansions

At low temperatures the lowest energy levels are dominant in determining the behavior of the system. Thus one could begin, as did Oguchi[14] for a ferromagnet, and evaluate g_c and E_c for the ground state and first few excited states. It is difficult, however, to obtain a sufficient number of terms to assure a rapid convergence of the series as the temperature is raised to the transition temperature. Thus Sykes and Fisher[15,16] have used various means to extrapolate from a finite number of terms to an infinite series. They have carried out calculations for the plane square and honeycomb two-dimensional lattices[15] and simple cubic and body-centered cubic three-dimensional lattices.[16] These series expansions are listed in Appendix A. It was felt that this was necessary since the original references have many annoying errors which have here been corrected.

3. High-temperature series expansions

If one desires to find an expansion which is valid at high temperatures clearly one must use a variable which goes to zero as T approaches infinity. Oguchi[17] has shown that a convenient expansion for the parallel susceptibility can be put in the form

$$\chi_{\parallel} = \frac{N\mu^2}{kT} \sum_{r=0}^{\infty} a_r v^r \quad , \tag{3.31}$$

where

N = the number of magnetic ions with magnetic moment equal to μ,

$v = \tanh(J/kT)$,

$a_o = 1$,

a_r = twice the term linear in N in the number of ways of placing r lines which connect neighboring sites on a lattice of N sites such that two sites in the lattice will be the meeting point of an odd number of lines.

The problem of evaluating the coefficients a_r is studied in more detail by Sykes.[18] Again it soon becomes difficult and impractical to calculate any but the first ten or so coefficients. Sykes and Fisher[15,16] have extrapolated the available series and extended the region of validity down to the transition temperature where the results of the low-temperature series and high-temperature series most agree. The corrected high temperature series expansions are listed in Appendix A for the four lattices previously mentioned.

4. Discussion of the Results of Sykes and Fisher

Table 3 lists some representative values of $\chi_{\parallel}(T)$ as calculated from the series listed in Appendix A. Figures 6-9 show graphically the behavior of $\chi_{\parallel}(T)$ for the four lattices considered by Sykes and Fisher. A comparison of these curves with the results of the molecular field approximation shows

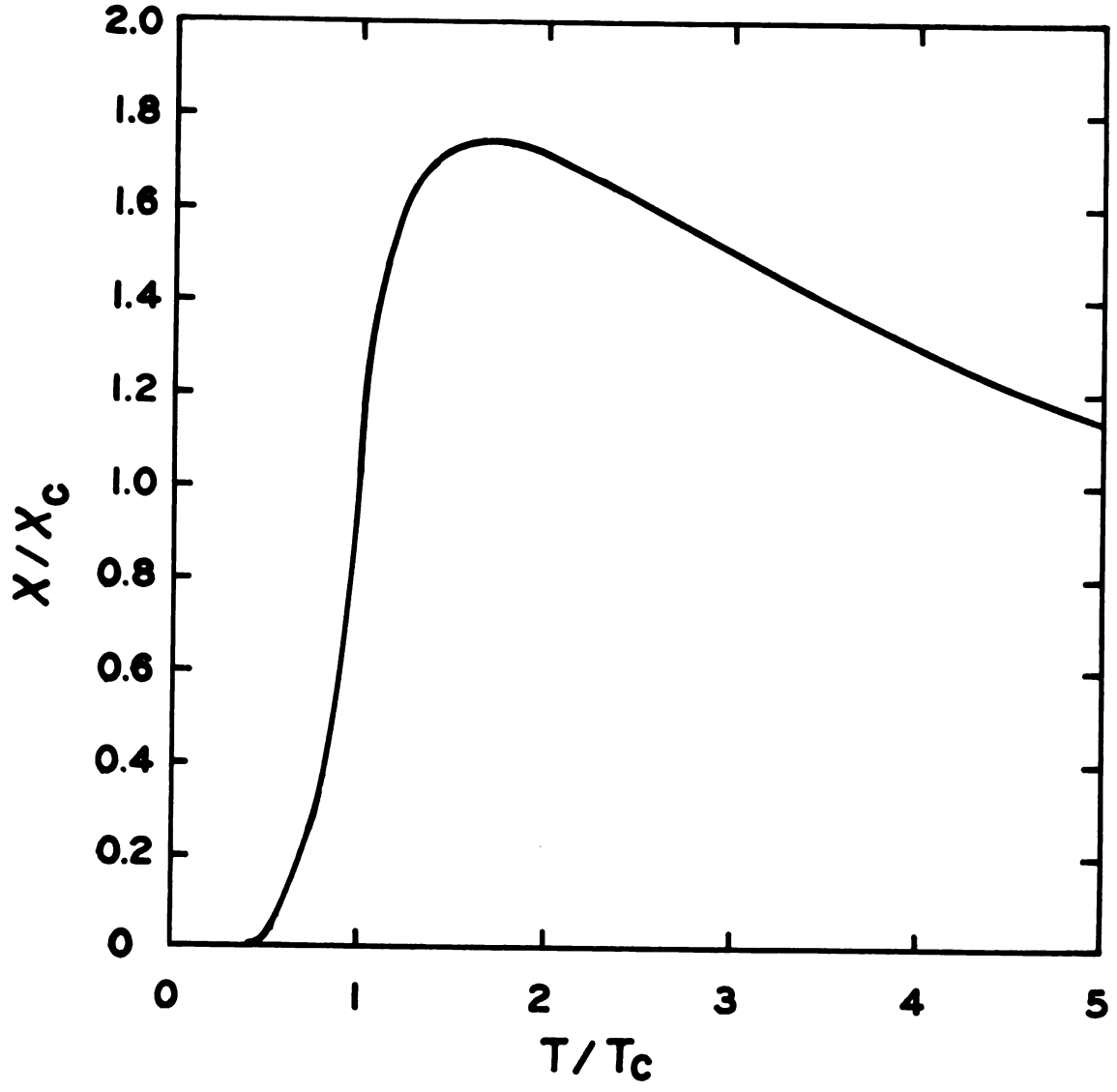

Fig. 6. χ/χ_c vs. T/T_c for two dimensional honeycomb Ising lattice.

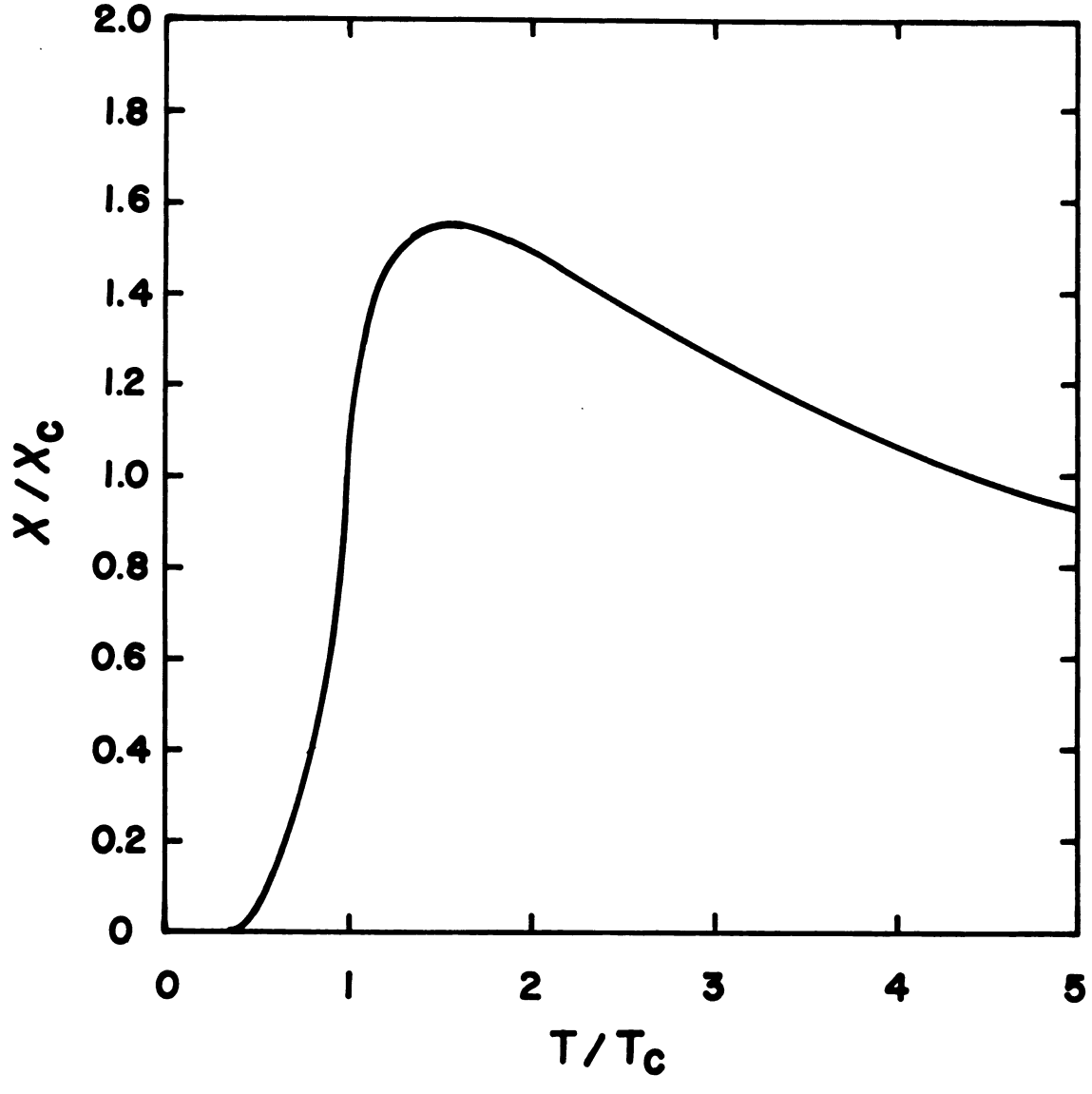

Fig. 7. χ/χ_c vs. T/T_c for two-dimensional plane square Ising lattice.

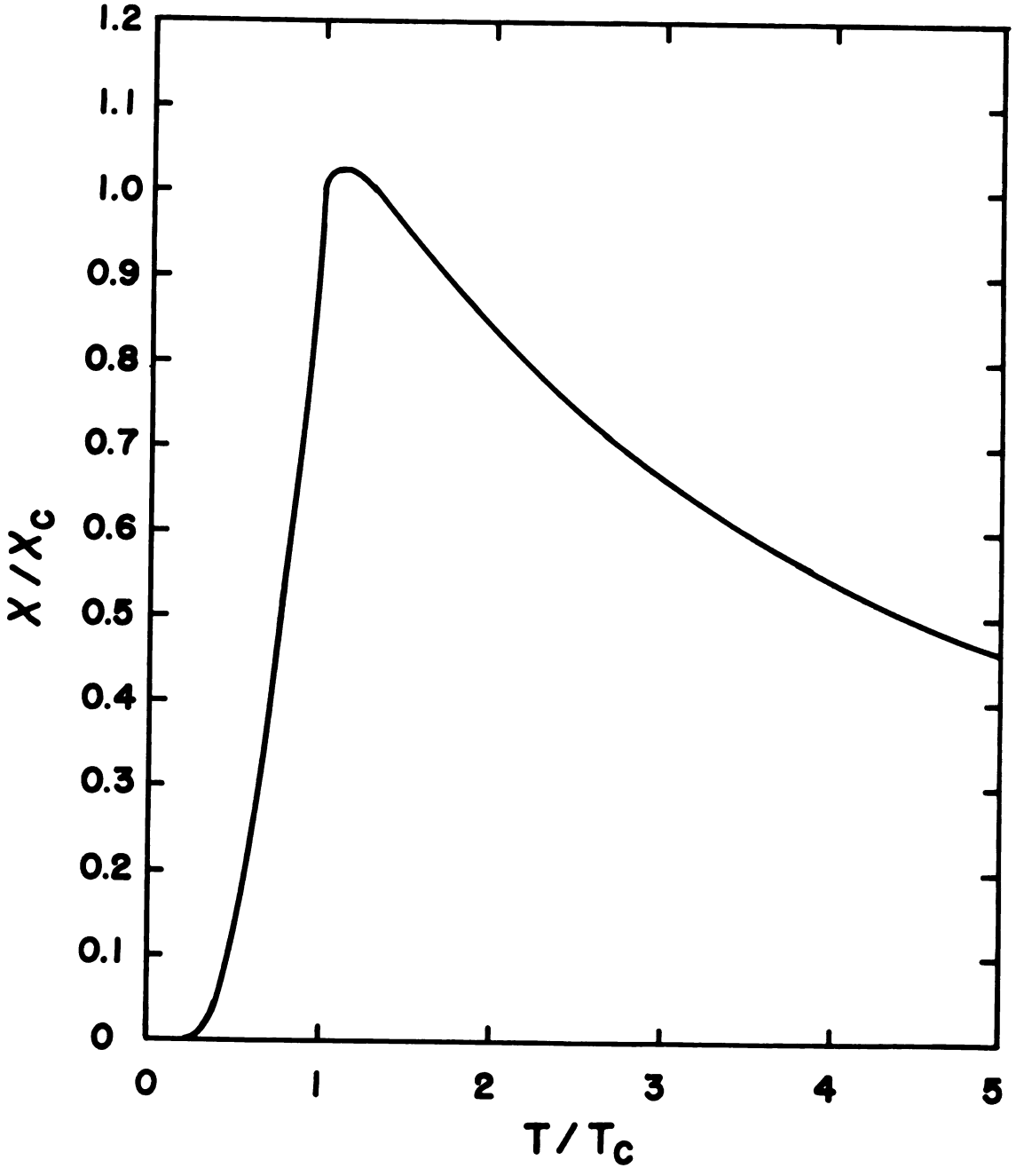

Fig. 8. χ/χ_c vs. T/T_c for three-dimensional simple cubic Ising lattice.

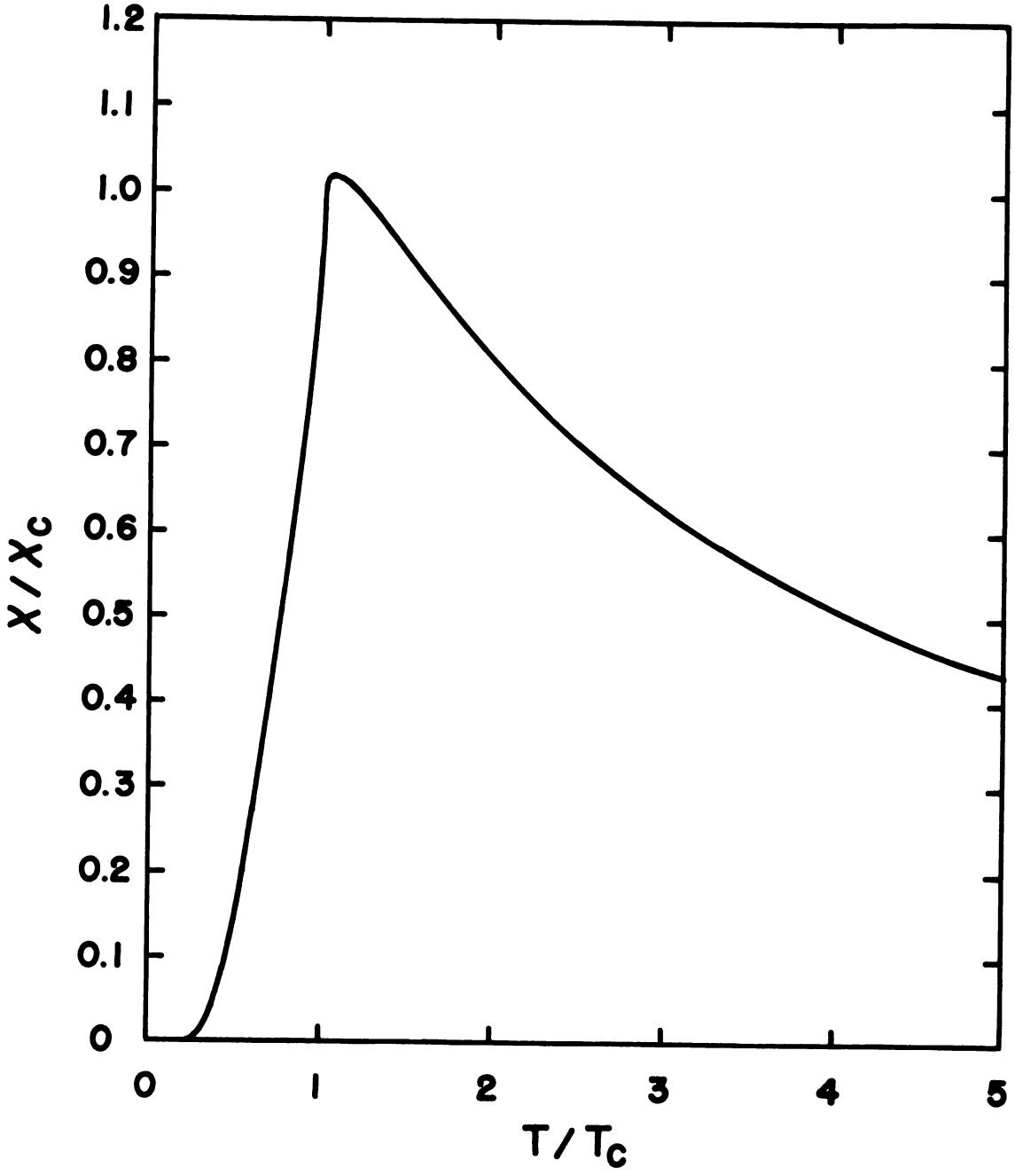

Fig. 9. χ/χ_c vs. T/T_c for three-dimensional body centered cubic Ising lattice.

some interesting differences. The molecular field approximation, which considers only long range ordering, results in a parallel susceptibility which has a very sharp peak at the transition temperature, with a discontinuity in the derivative of χ with respect to T. On the other hand, the Ising model, which considers both short and long-range ordering, gives rise to a rounded peak in the susceptibility at a temperature slightly above the transition temperature, which is characterized by a vertical inflection point in the susceptibility. The difference in the nature of the peak in $\chi_{\parallel}$ is, I feel, mainly a result of the way in which short-range order is treated. In the molecular field approach each spin is considered to be interacting with the average magnetization of each sublattice, ignoring the effects of local fluctuations, while the Ising model considers each spin to be interacting with its nearest neighbors, which allows both short and long-range effects to be considered. Short-range effects must be considered near the transition temperature where fluctuations are large.

A comparison of Figs. 6-9 among themselves shows that the differences <u>within</u> the two-dimensional and three-dimensional lattices is small, while there is a more striking difference <u>between</u> the two and three-dimensional lattices. Both two-dimensional lattices have their transition temperature considerably below a very broad peak in the parallel susceptibility while both three-dimensional lattices have

their transition temperature only slightly below a more sharply rounded peak in $\chi_{\parallel}$. Thus dimensionality plays a more important role than do differences among lattices of the same dimension.

IV. EXPERIMENTAL RESULTS AND DISCUSSION

A. $Co(tu)_4Cl_2$

$Co(tu)_4Cl_2$ forms crystals with tetragonal point symmetry 4/m. From the x ray data available it is found that the unit cell dimensions are a = 13.52 A and c = 9.10 A with four formula units per unit cell, and that the space group is $P4_2/n$.

Magnetic susceptibility measurements were made on several single crystals and powdered samples of $Co(tu)_4Cl_2$ in the temperature range 0.45°K to 4.2°K. The sample weight was in the range of 1.0 to 1.5 grams. The experimental data is given numerically in Tables 4-7 in Appendix B and shown graphically in Figs. 10 and 11. Figure 10 shows the susceptibility data taken for the [001], [100], and [110] axes. From this data it is deduced that this material is antiferromagnetically ordered below T = 0.93°K and that the sublattice magnetization vectors lie along or very near to the c axis.

The antiferromagnetic transition temperature is defined as the temperature at which $d(\chi_{\parallel} T)/dT$ assumes its maximum value.[19] In Fig. 12 this quantity has been plotted as a function of temperature. There is an asymmetrical but well-defined peak at T = 0.93°K indicating that this is indeed

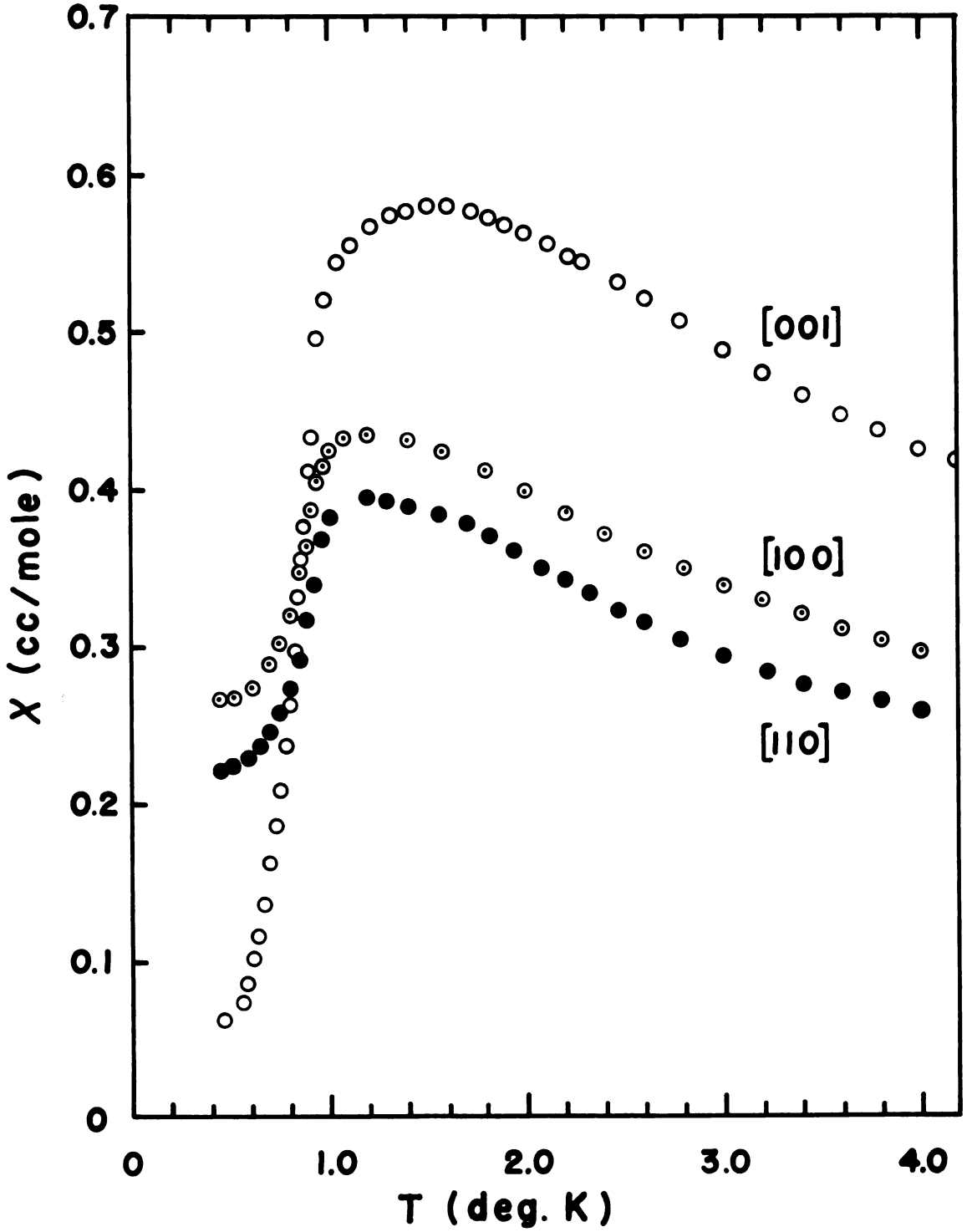

Fig. 10. Magnetic susceptibility of $Co(tu)_4Cl_2$ along the [001], [100] and [110] axes.

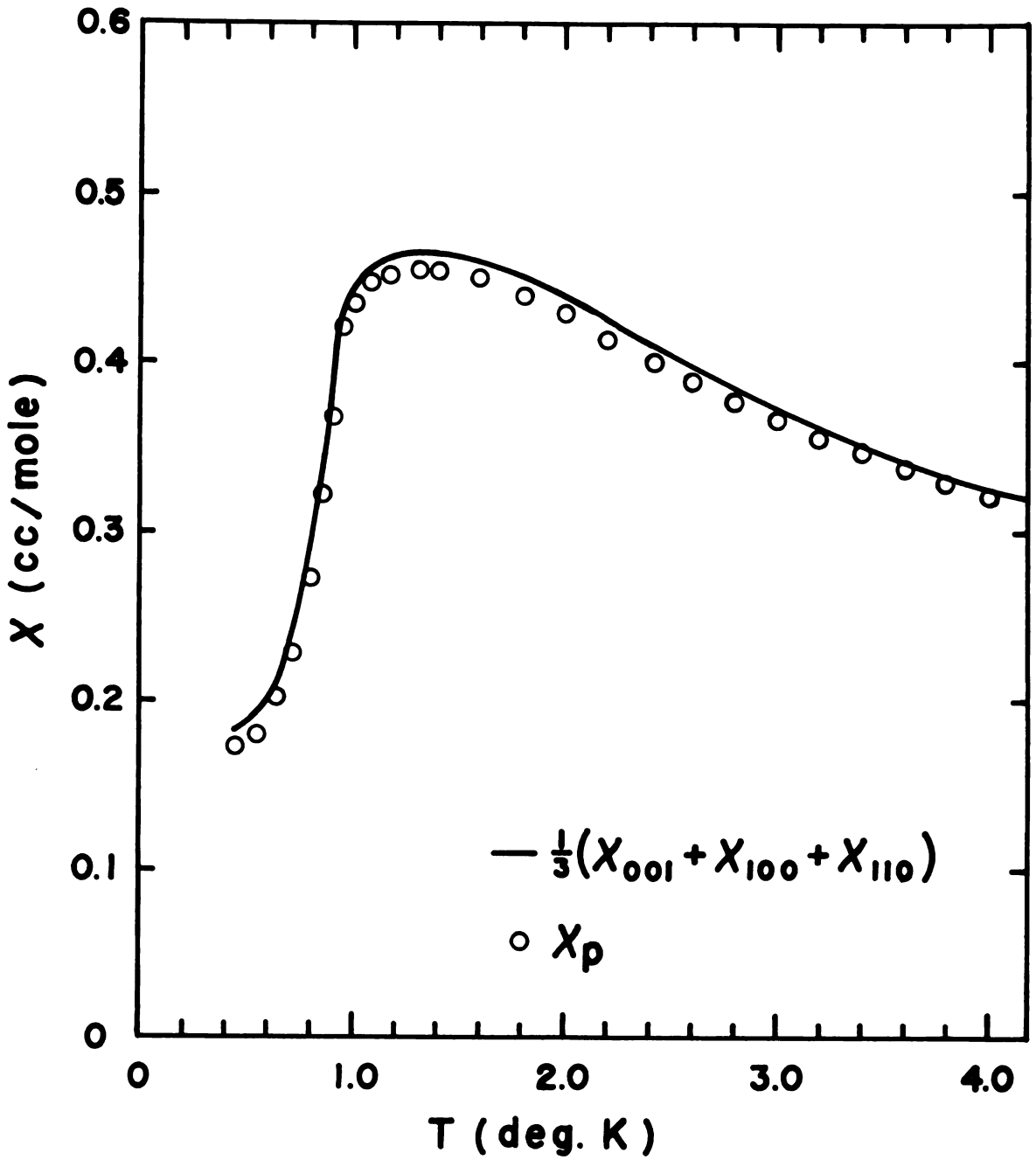

Fig. 11. Magnetic susceptibility of $Co(tu)_4Cl_2$ powder compared to $\frac{1}{3}(\chi_{001} + \chi_{100} + \chi_{110})$.

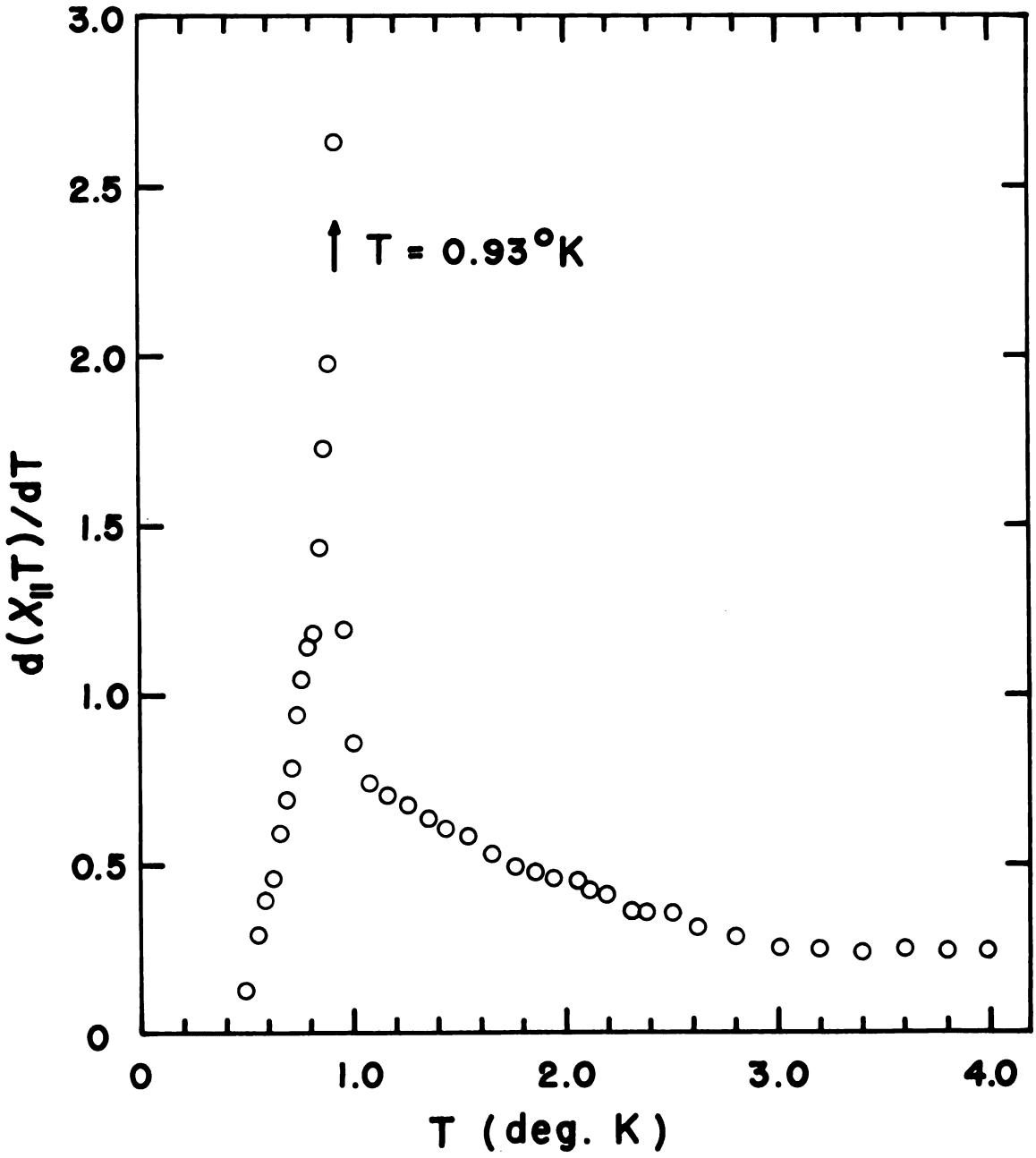

Fig. 12. Plot of $d(\chi_{\parallel}T)/dT$ for $Co(tu)_4Cl_2$.

the correct value for the transition temperature of $Co(tu)_4Cl_2$. This is confirmed by proton magnetic resonance experiments which indicate that this is the temperature at which local internal magnetic fields begin to appear at the proton sites.

The conclusion that the sublattice magnetization vectors lie along or near to the c axis is consistent with the results of the proton resonance investigation carried out by Spence et al. An exhaustive analysis of the proton resonance data leaves three possibilities for the magnetic symmetry group, two of which give the same sublattice structure for $Co(tu)_4Cl_2$. The possible spin arrangements are shown in Figs. 13 and 14. The cobalt ions are located at $(\frac{1}{4}, \frac{1}{4}, \frac{1}{4})$, $(\frac{3}{4}, \frac{3}{4}, \frac{1}{4})$, $(\frac{1}{4}, \frac{3}{4}, \frac{3}{4})$, and $(\frac{3}{4}, \frac{1}{4}, \frac{3}{4})$ respectively in each chemical unit cell. In Fig. 13 the magnetic unit cell is identical to the chemical unit cell, while in Fig. 14 the magnetic unit cell is twice the size of the chemical unit cell, being elongated along the c axis.

If one could make some predictions, based on the details of the crystal structure and the nature of indirect exchange interactions, about the magnitude and sign of the exchange integral between various neighboring cobalt ions one could possibly decide which of these spin arrangements is most likely correct. The program of calculation is fairly straightforward.

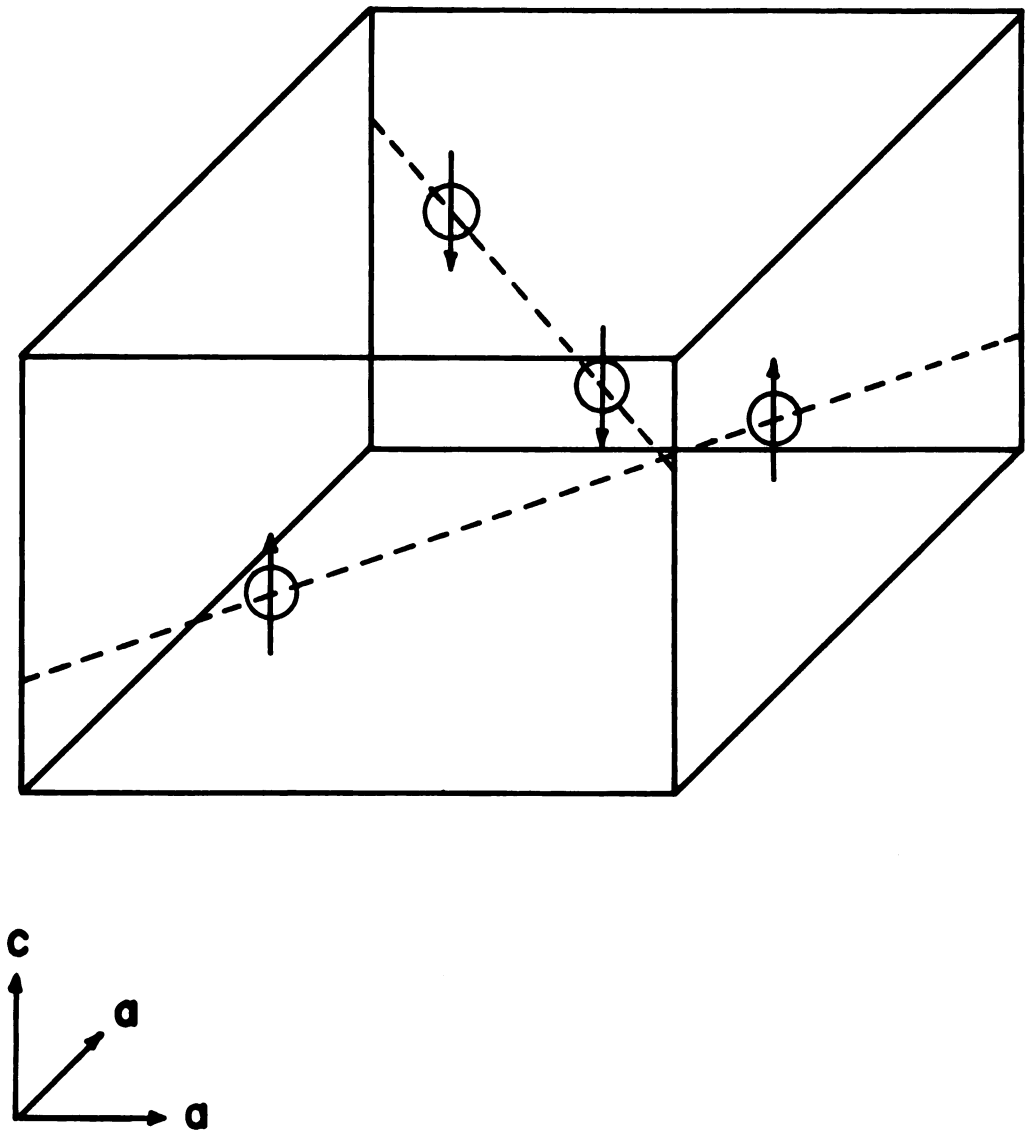

Fig. 13. Possible spin arrangement for $Co(tu)_4Cl_2$ having the symmetry $P\,4'_2/n$ or $P\,4'_2/m$.

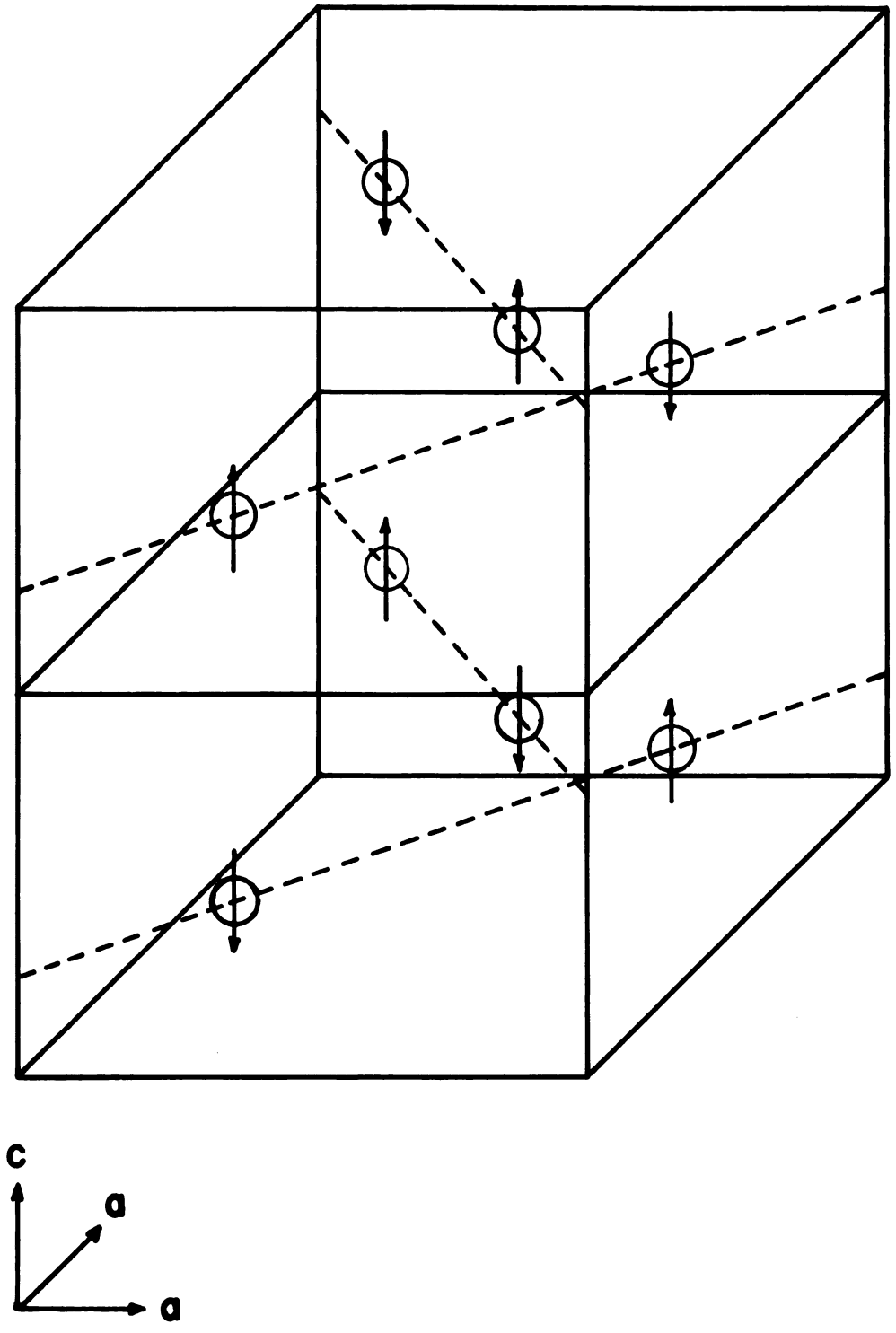

Fig. 14. Possible spin arrangement for $Co(tu)_4Cl_2$ having the symmety I_c4_1.

1. For each spin arrangement calculate the ground state energy E.

2. If one of these ground state energies is obviously lower than the other the problem is solved. If there is uncertainty or if a check is desired go to step (3).

3. For each spin arrangement calculate the susceptibility at T = 0°K by minimizing the quantity $E - \vec{M}\cdot\vec{H}$ with respect to deviations in the direction of the sublattice magnetizations. This calculated susceptibility will be a function of the values of the various exchange integrals.

4. From the measured values of the susceptibility calculate the values of the exchange integrals by requiring agreement between measured and calculated values of the susceptibility for each spin arrangement.

5. Compare the sets of exchange integrals calculated from (4) with the initial predictions and choose the spin arrangement which leads to the most consistent results.

Unfortunately, at this time there is not yet enough information available upon which to base predictions concerning the values of the various exchange integrals. Hence, the program outlined above cannot yet be carried out.

It has long been customary to compare the behavior of the magnetic susceptibility above the transition temperature with the Curie-Weiss law, $\chi = C/(T + \theta)$, based on the molecular field approximation. Figure 15 shows that within the limited temperature range of 2°K to 4°K the powder

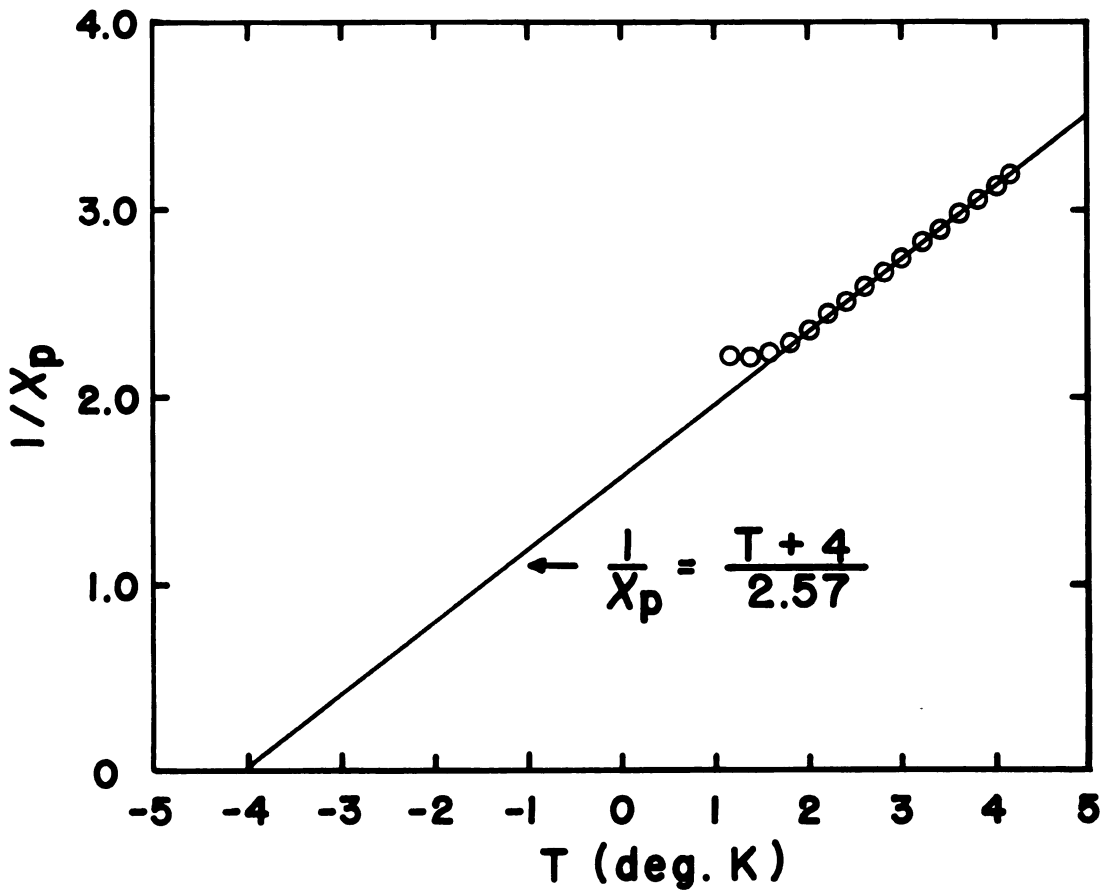

Fig. 15. Curie-Weiss behavior of $Co(tu)_4Cl_2$.

susceptibility obeys the relation $\chi_p = 2.57/(T + 4°K)$. If one were interested in a more critical comparison with the Curie-Weiss law more data above 4.2°K would be needed.

In Figs. 16-18 the c axis susceptibility of $Co(tu)_4Cl_2$ is compared to some of the results of the Ising model calculations. Figures 16 and 17 show the comparison with the two-dimensional honeycomb and plane square lattices where the data has been normalized to $T_c = 0.93°K$ and the maximum susceptibility equal to that of the Ising lattices. In each case there is agreement on general features but some differences in detail. The broad nature of the peak suggests a two-dimensional character of the exchange interactions. Possibly the exchange interactions within a set of planes in the lattice are large compared to interactions between planes, although this is not obvious from available structural information. In an attempt to obtain a better fit in the region of the transition temperature Fig. 18 shows a comparison with the honeycomb lattice where the data has now been normalized to $T_c = 0.85°K$. In the temperature range below 2°K the fit is indeed better, but this is somewhat illusory since $T_c = 0.93°K$, not 0.85°K.

A more serious difficulty brought out by these comparisons is the fact that at the low temperature extreme the experimental data begins to differ significantly from the theoretical curve and seems to indicate a non-zero value for the susceptibility at T = 0°K. This descrepancy may be

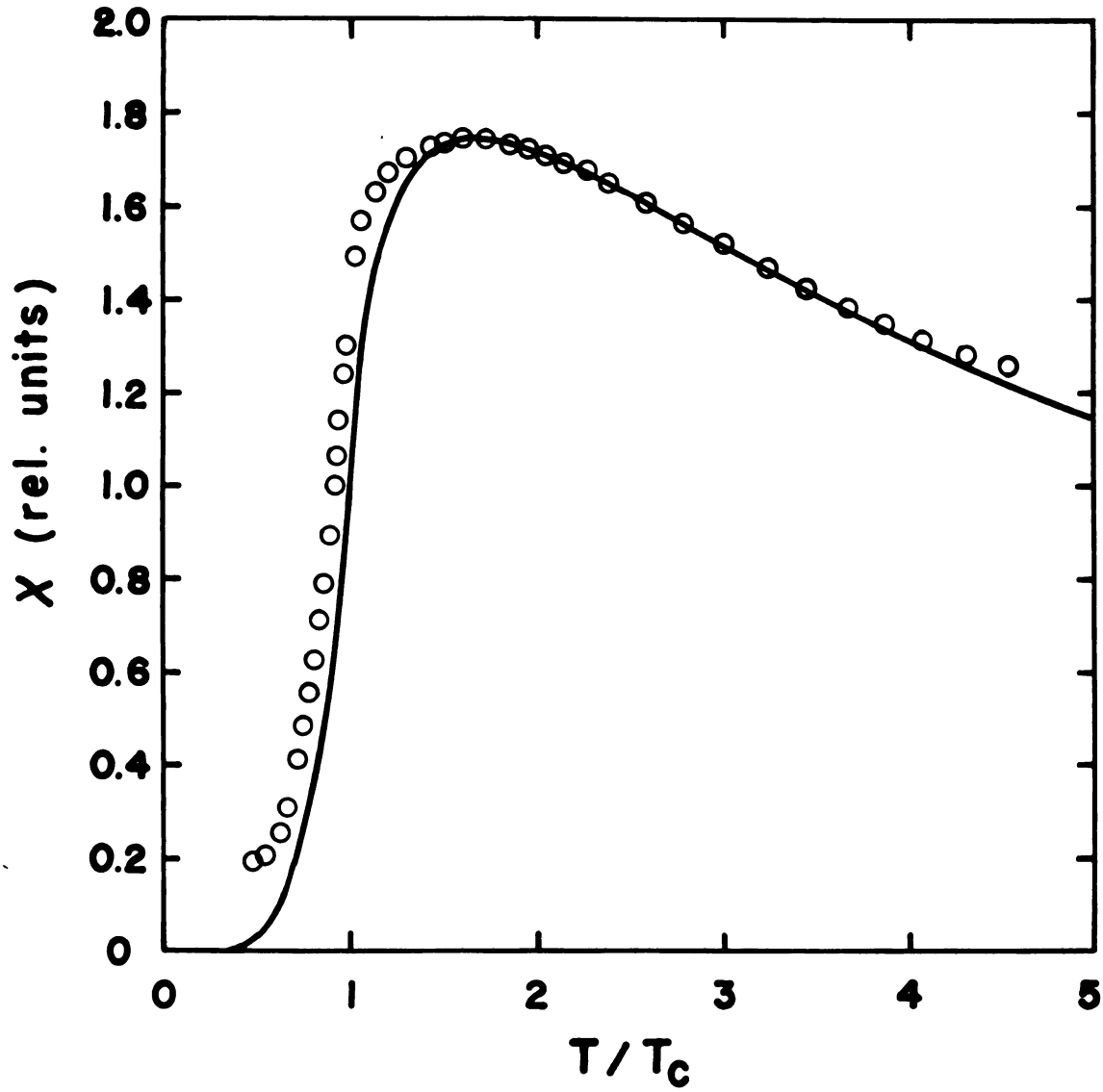

Fig. 16. Comparison of $\chi_{\parallel}$ for $Co(tu)_4Cl_2$ with honeycomb Ising lattice. The data points have been normalized to $T_c = 0.93^{\circ}K$ and $\chi_{max.} = 1.742$.

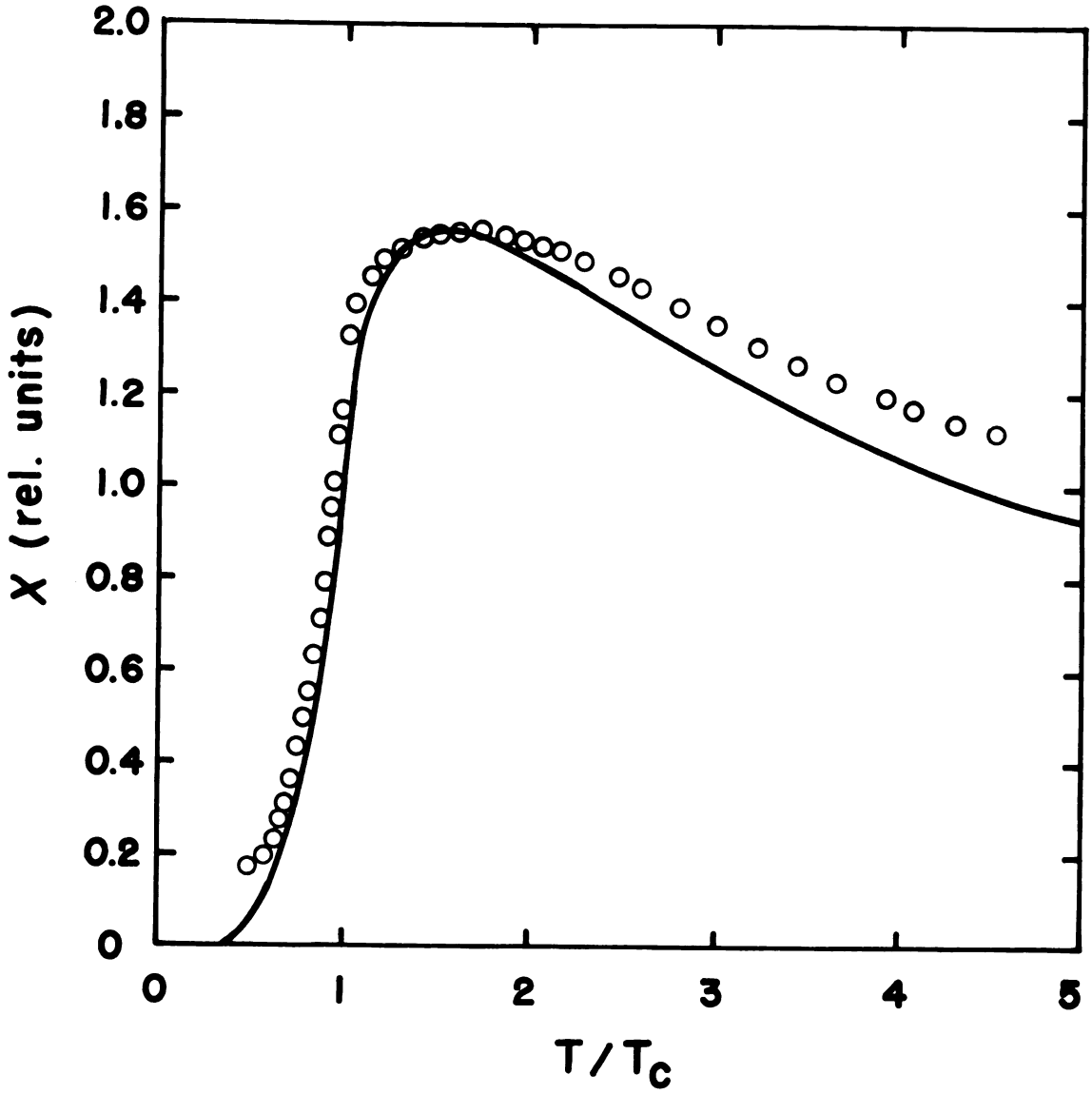

Fig. 17. Comparison of $\chi_{\parallel}$ for $Co(tu)_4Cl_2$ with plane square Ising lattice. The data points have been normalized to $T_c = 0.93°K$ and $\chi_{max.} = 1.552$.

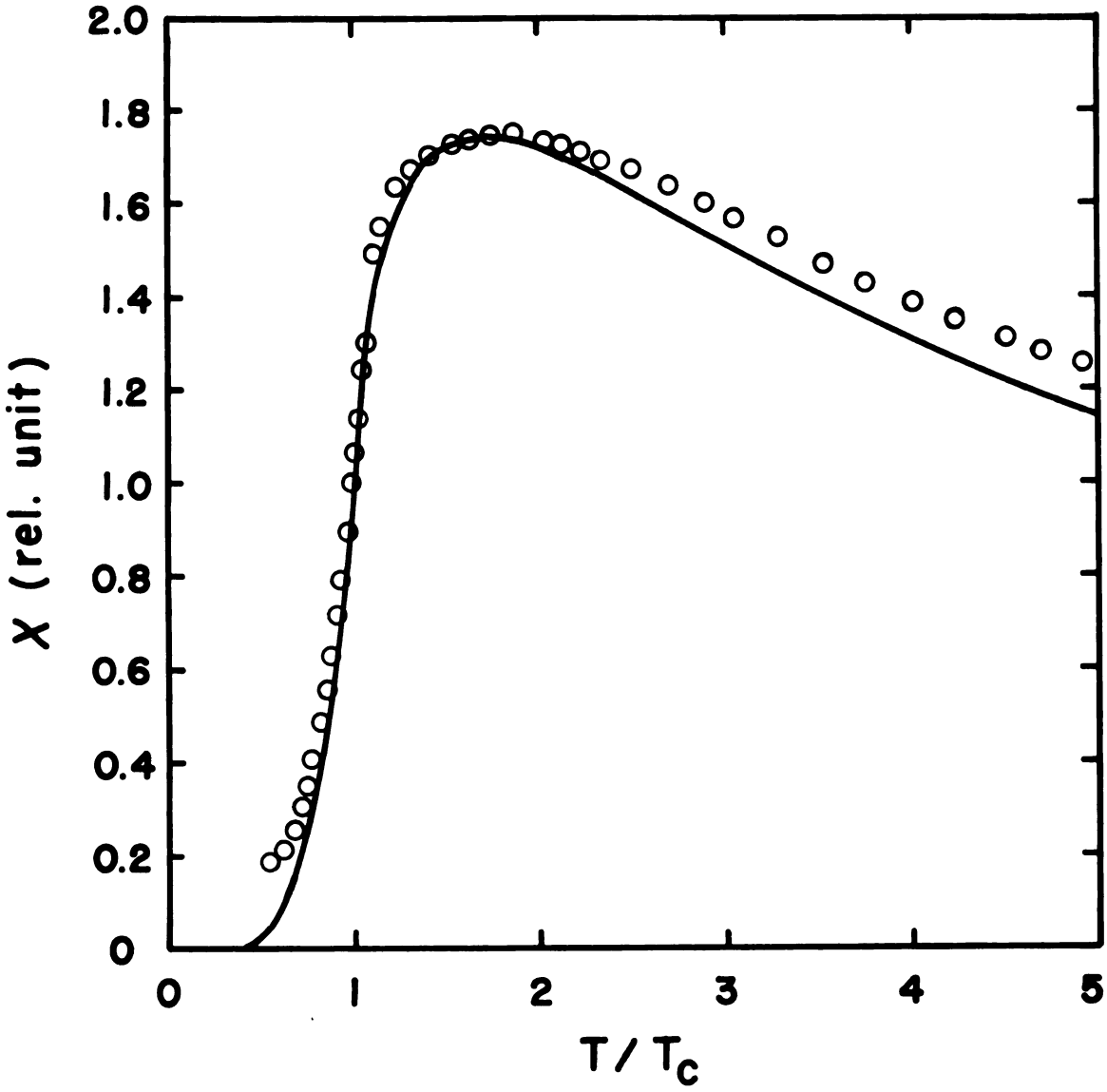

Fig.18. Comparison of $\chi_{\parallel}$ for $Co(tu)_4Cl_2$ with honeycomb Ising lattice. The data points have been normalized to $T_c = 0.85^{\circ}K$ and $\chi_{max.} = 1.742$.

due to experimental error, either in the value of the sample temperature or, more likely, in the value of M_o as calculated from Eq. (2.6). It might also be a real effect showing that a two-sublattice model is inadequate. In either case, measurements below 0.45°K would help resolve the difficulty.

It is hardly appropriate to try to draw any further conclusions from these comparisons since the Ising model, like any other model, is based on a set of simplifying assumptions which are not in general satisfied by any real crystal. However, the more satisfactory treatment of the statistical properties in the Ising model is certainly a great improvement over the molecular field approach. Further improvements in the theoretical treatment of an antiferromagnet will require a more realistic and complete Hamiltonian whose range of interaction extends over several lattice parameters, while retaining a rigorous statistical treatment.

B. $Mn(tu)_4Cl_2$

$Mn(tu)_4Cl_2$ forms crystals with tetragonal point symmetry 4/m similar in habit to $Co(tu)_4Cl_2$. X ray data indicates that it has the space group $P4_2/n$ with four chemical formula units per unit cell of dimensions a = 13.76 A and c = 9.07 A.

Figure 19 displays the results of measurements of the magnetic susceptibility along the [001], [100], and [110]

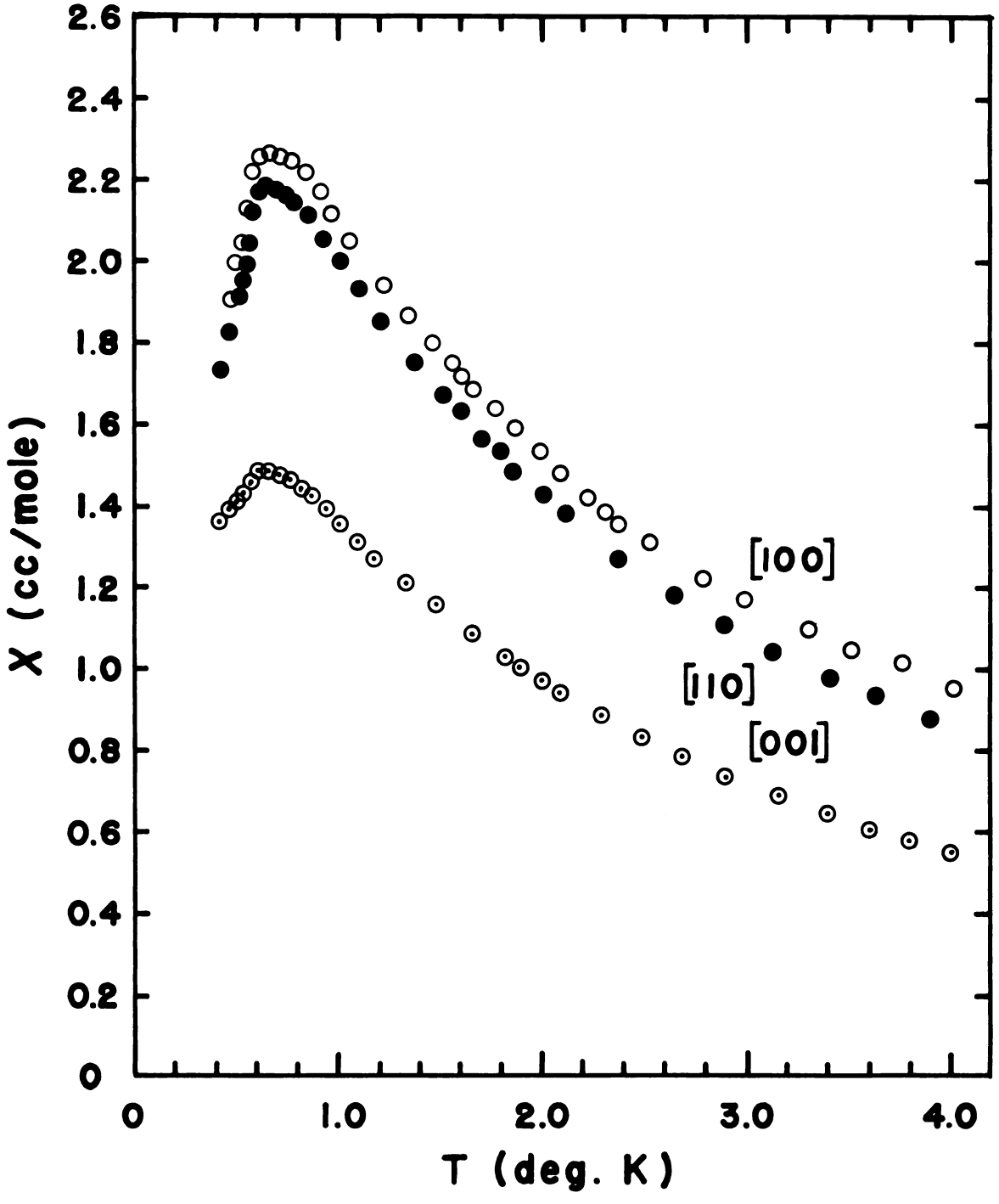

Fig. 19. Magnetic susceptibility of $Mn(tu)_4Cl_2$ along the [001], [100], and [110] axes.

axes. The numerical data is listed in Tables 8-10 in Appendix B. The general features of Fig. 19 indicate that $Mn(tu)_4Cl_2$ undergoes an antiferromagnetic transition at $T = 0.56°K$. However, the sublattice magnetization vectors do not appear to lie near the c axis as in $Co(tu)_4Cl_2$. In fact, the c axis data indicates that the sublattice magnetization vectors probably lie close to the ab plane.

If one considers a simple two-sublattice model with the sublattice magnetization vectors lying in the ab plane it must be noted that these vectors could lie along either of two equivalent axes which are at right angles to each other. Thus, the possibility of domains would have to be considered. If the volume of each type of domain were equal then the susceptibility in the ab plane would, in the first approximation, be isotropic and equal to $\frac{1}{2}(\chi_{\parallel} + \chi_{\perp})$. The susceptibility along the c axis would be $\chi_{\perp}$.

Following this model a little further, Fig. 20 shows a plot of $\chi_{\parallel}(T)$ where $\chi_{\parallel} = (\chi_{100} + \chi_{110}) - \chi_{001}$. Figures 21 and 22 show a comparison of this $\chi_{\parallel}$ with the three-dimensional simple cubic and two-dimensional plane square lattices. In each case the fit is poor but the three-dimensional case seems to be preferred, in contrast with $Co(tu)_4Cl_2$ which fit reasonably well with the two-dimensional results. Figure 23 shows a plot of $d(\chi_{\parallel}T)/dT$ to demonstrate that $T_c = 0.56°K$ and to show the expected behavior of the magnetic contribution to the specific heat.

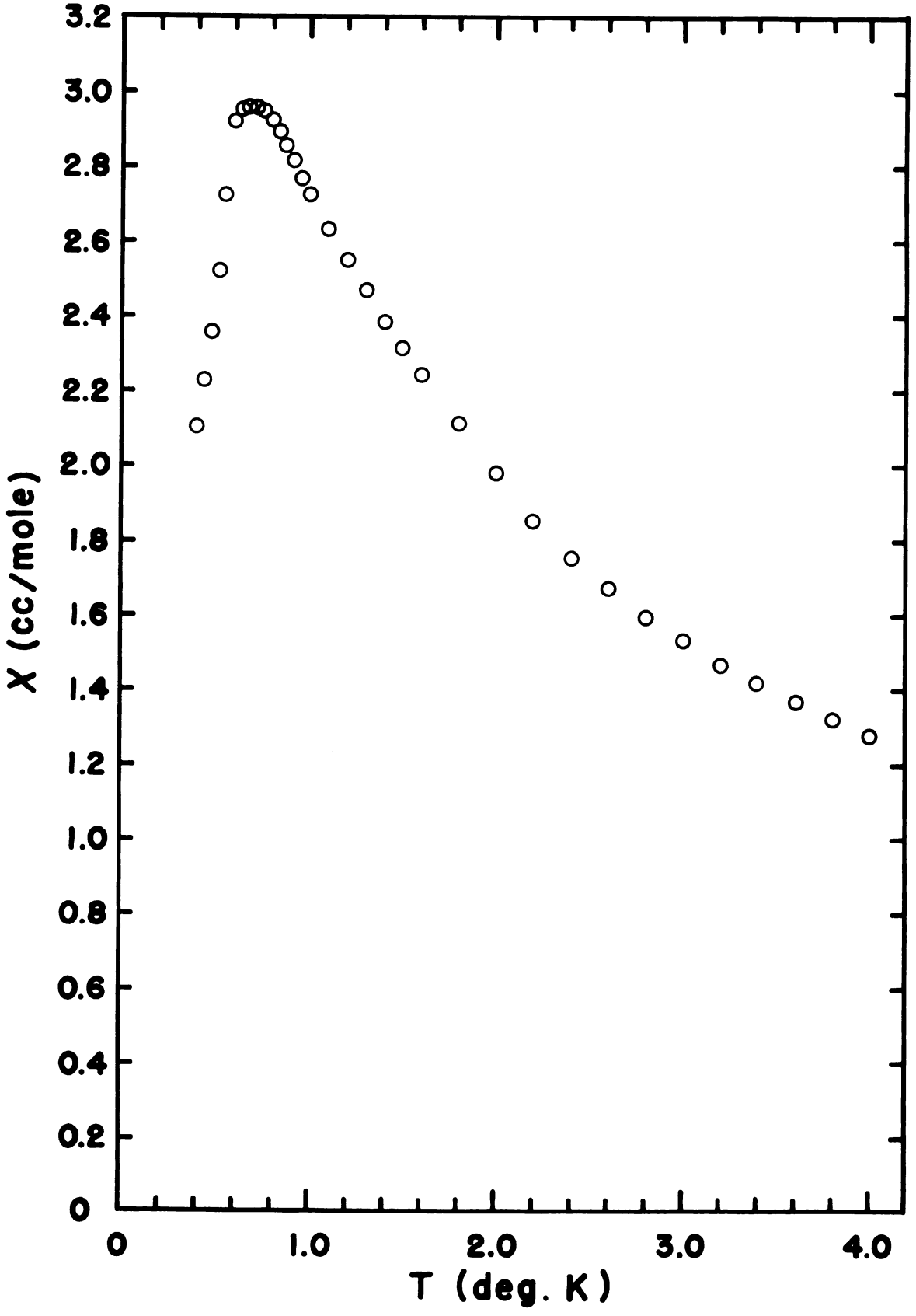

Fig. 20. Plot of $\chi_{\parallel}(T)$ for $Mn(tu)_4Cl_2$.

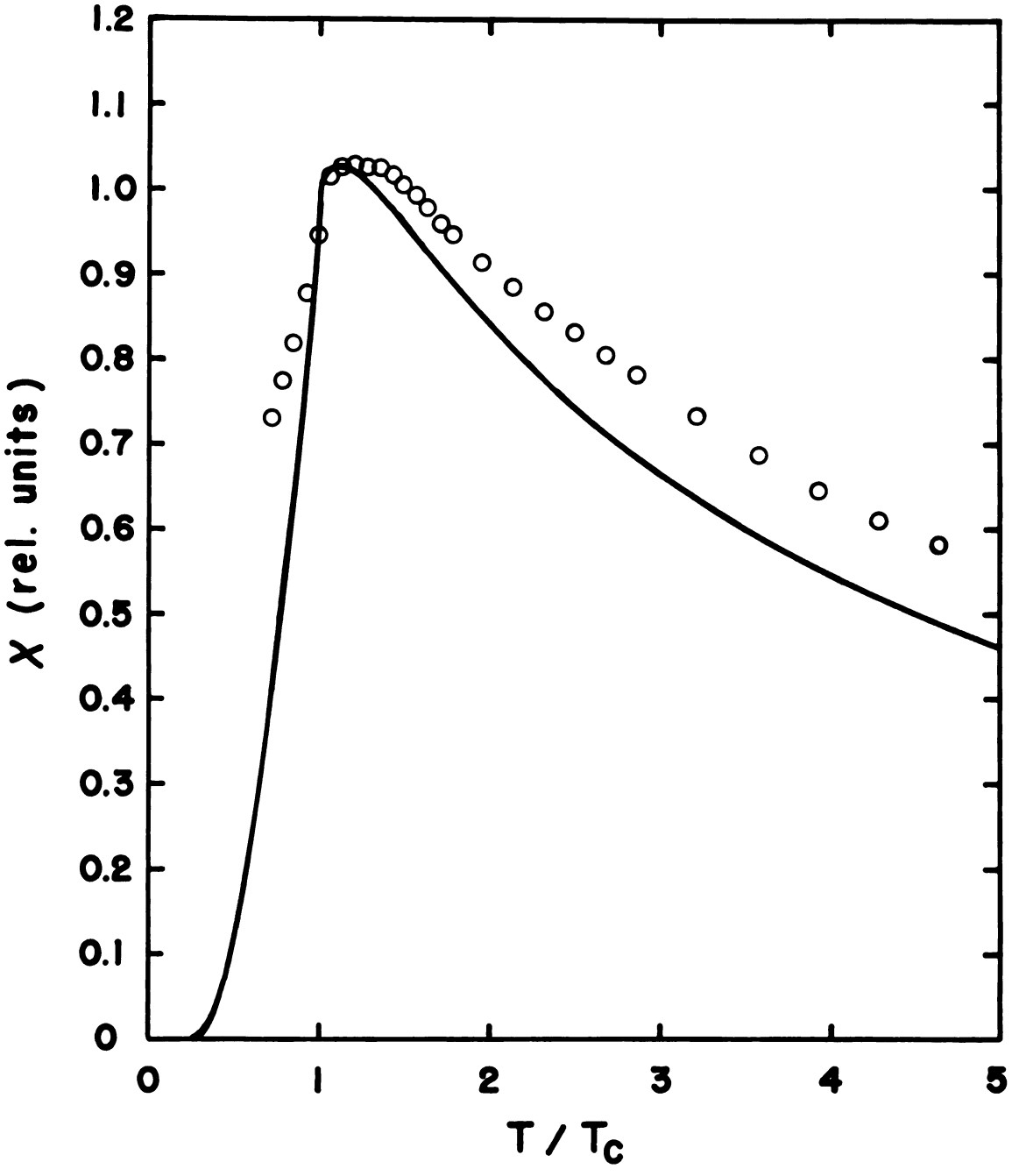

Fig.21. Comparison of $\chi_{\parallel}$ for $Mn(tu)_4Cl_2$ with the three-dimensional simple cubic Ising lattice .

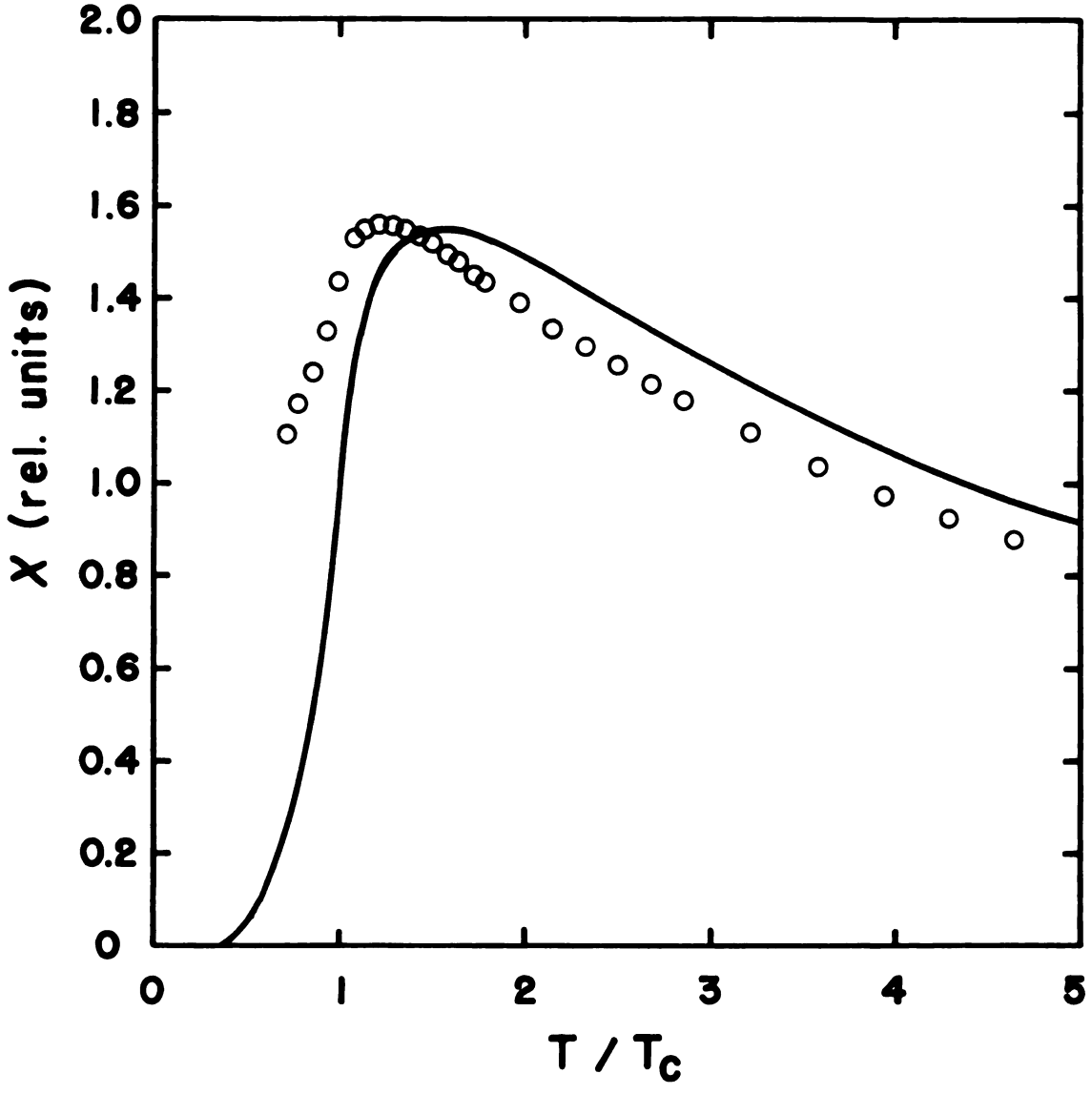

Fig. 22. Comparison of $\chi_{\parallel}$ for $Mn(tu)_4Cl_2$ with the plane square Ising lattice. The data has been normalized to $T_c = 0.56^{\circ}K$ and $\chi_{max.} = 1.552$.

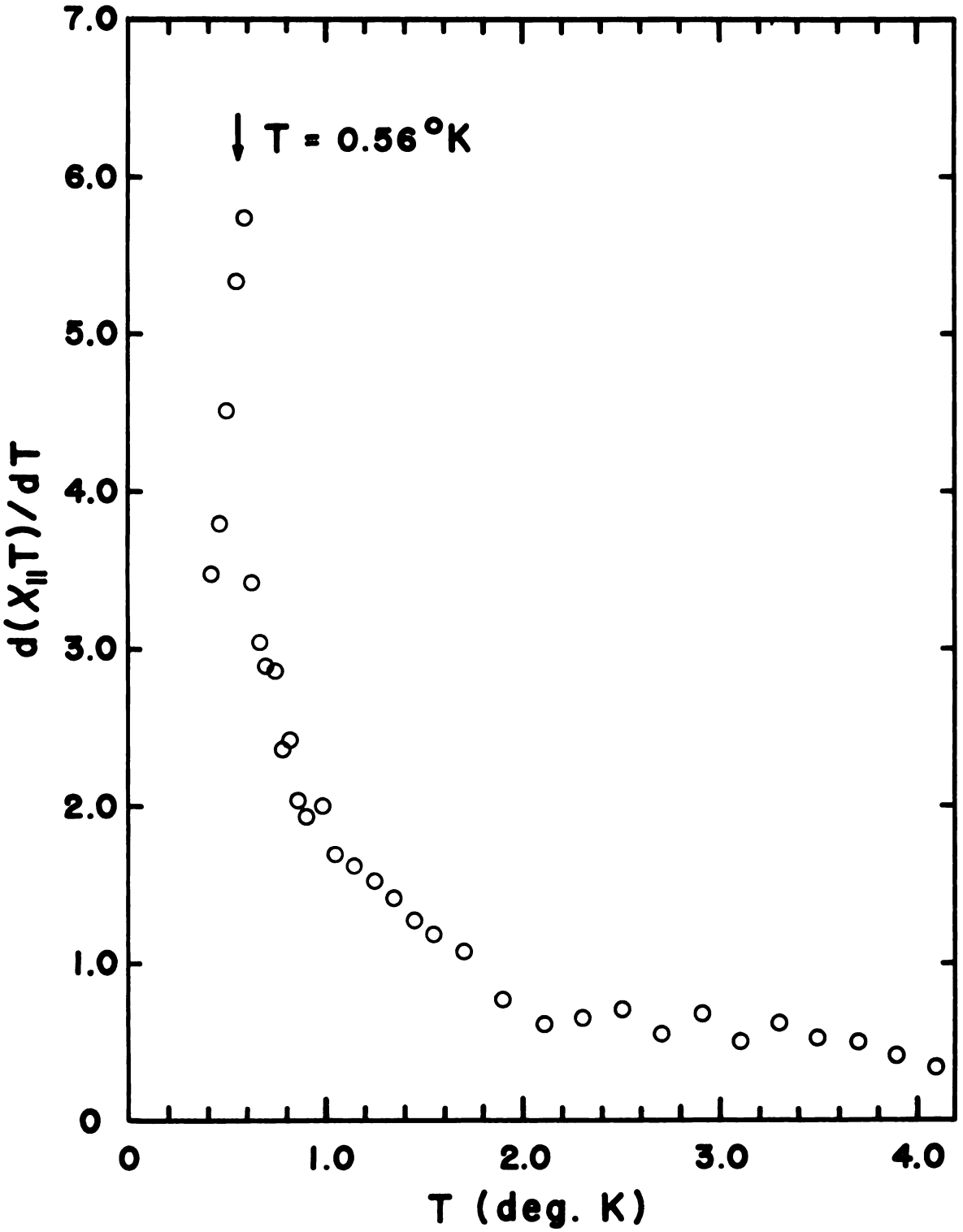

Fig. 23. Plot of $d(\chi_{||}T)/dT$ for $Mn(tu)_4Cl_2$.

There is, however, an annoying problem with the $\chi_{\parallel}$ as calculated. It appears that our $\chi_{\parallel}$ will have a non-zero value at T = 0°K. This could be the result of errors in the temperature measurements but such large errors are not expected. More likely possibilities are that a simple two-sublattice model is inadequate or that χ_{001} is significantly different from the $\chi_{\perp}$ in the ab plane. In either case measurements at much lower temperatures are required to resolve the problem.

No susceptibility measurements were made on powdered samples. However, χ_p is estimated to be equal to $\frac{1}{3}(\chi_{100} + \chi_{110} + \chi_{001})$. Figure 24 shows a comparison of the χ_p with the Curie-Weiss law $\chi_p = \frac{4.05}{T + 1.1}$.

C. $Ni(tu)_6Br_2$

1. Introduction

Of the three materials investigated in this project thiourea-coordinated nickel bromide, $Ni(tu)_6Br_2$, has the most interesting behavior. The two features of special interest are that: (1) along no axis does the magnetic susceptibility approach zero at low temperatures; (2) both the magnetic susceptibility data and specific heat data indicate that there are two distinct transitions at 2.0°K and 2.2°K respectively. These features will be demonstrated in the following graphic and tabular presentation of the experimental data.

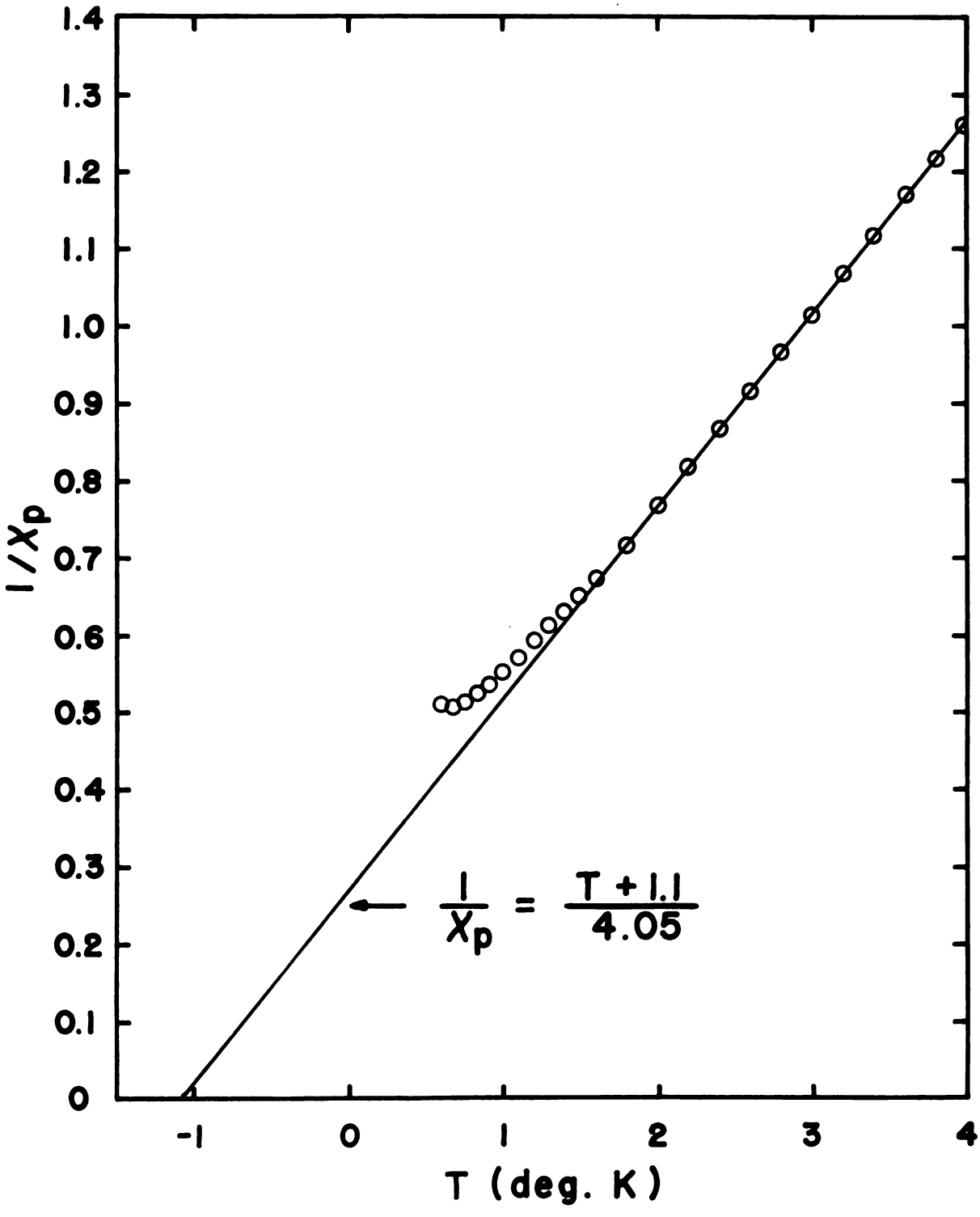

Fig.24. Curie-Weiss behavior of χ_p for $Mn(tu)_4Cl_2$. $\chi_p = \frac{1}{3}(\chi_{001} + \chi_{100} + \chi_{110})$.

2. Presentation of Data

A preliminary x ray diffraction study of $Ni(tu)_6Br_2$ indicates that it has monoclinic point symmetry 2/m, space group C2/c, with four formula units per unit cell of dimensions a = 24.30A, b = 8.91A, c = 16.79A, and $\beta = 137.02°$. Figure 25 shows the appearance of a typical single crystal as viewed along the b axis, and indicates the other directions of interest in the ac plane. Single-crystal susceptibility measurements were made along the a, a', f, c, and b directions. Susceptibility data was also taken on powdered samples.

Tables 11-13 of Appendix B give the data for measurements of the susceptibility along the b, a', and c directions. This is shown in graphic form in Fig. 26. A very careful observation of the c axis data will show inflection points in χ vs. T at T = 2.0°K and T = 2.2°K respectively. This feature will be more clearly seen in Fig. 32 to be described later. Note also that the b axis, which by symmetry considerations must be a magnetic principal axis, exhibits a magnetic susceptibility which increases below T = 2.2°K and approaches a maximum value of approximately 0.092 cc/mole as $T \rightarrow 0°K$.

Tables 14 and 15 list the experimental points shown graphically in Fig. 27 which exhibits the behavior of the magnetic susceptibility along the f and a directions of $Ni(tu)_6Br_2$. Again, a careful study of the behavior of

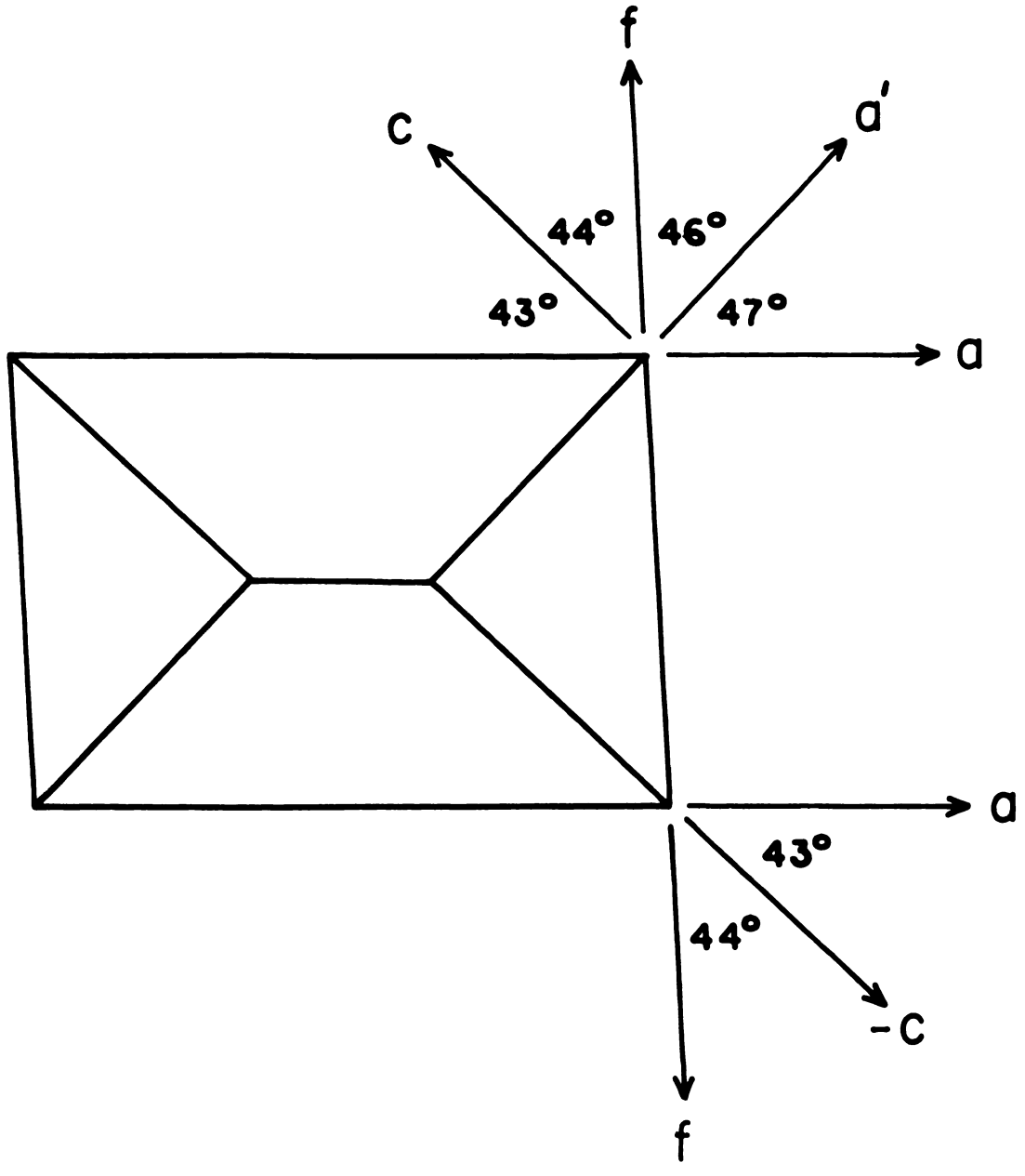

Fig. 25. Identification of directions in the ac plane of $Ni(tu)_6Br_2$. The b axis points directly into the plane of this page.

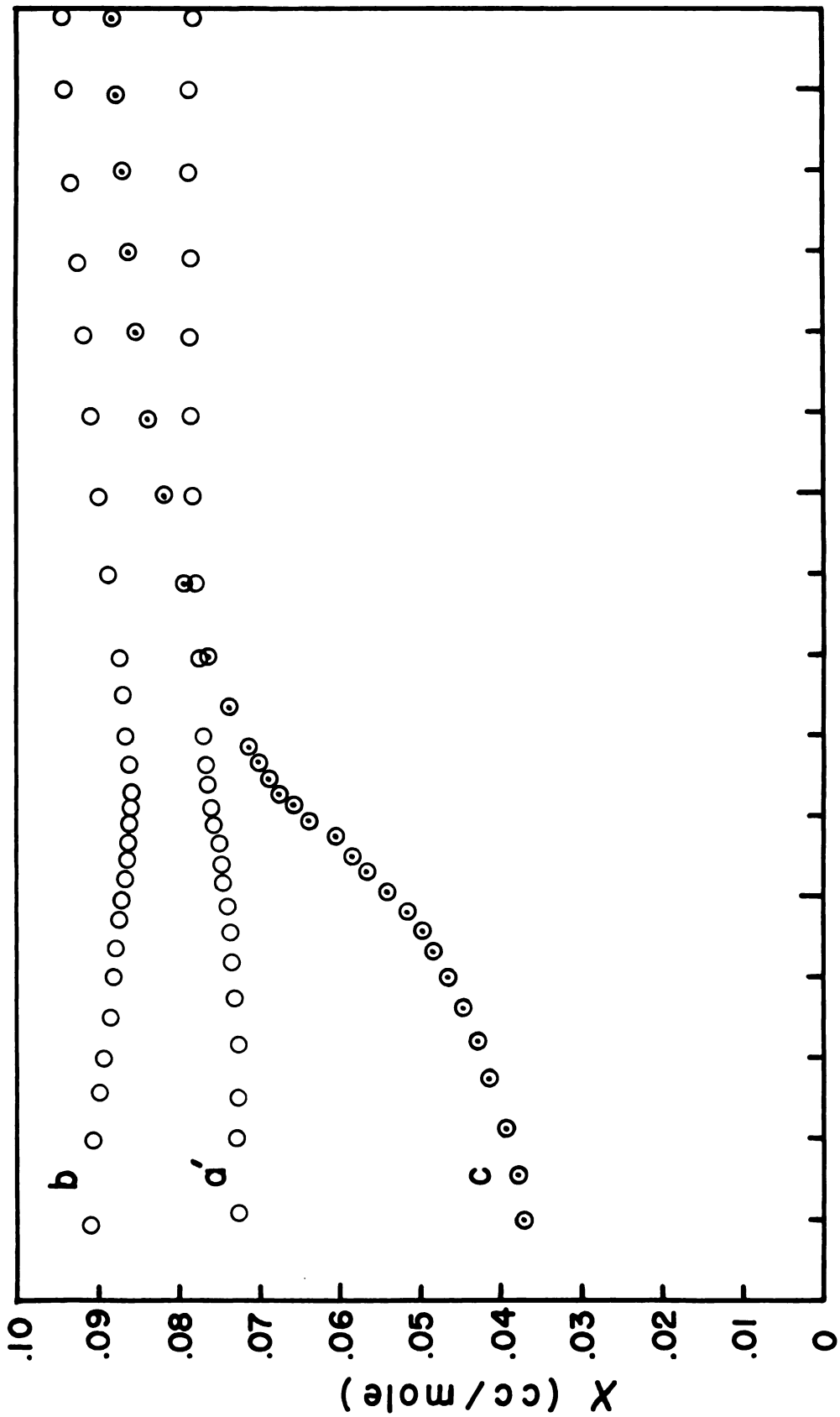

Fig. 26. Magnetic susceptibility of $Ni(tu)_6Br_2$ vs. temperature along the b, d′ and c directions.

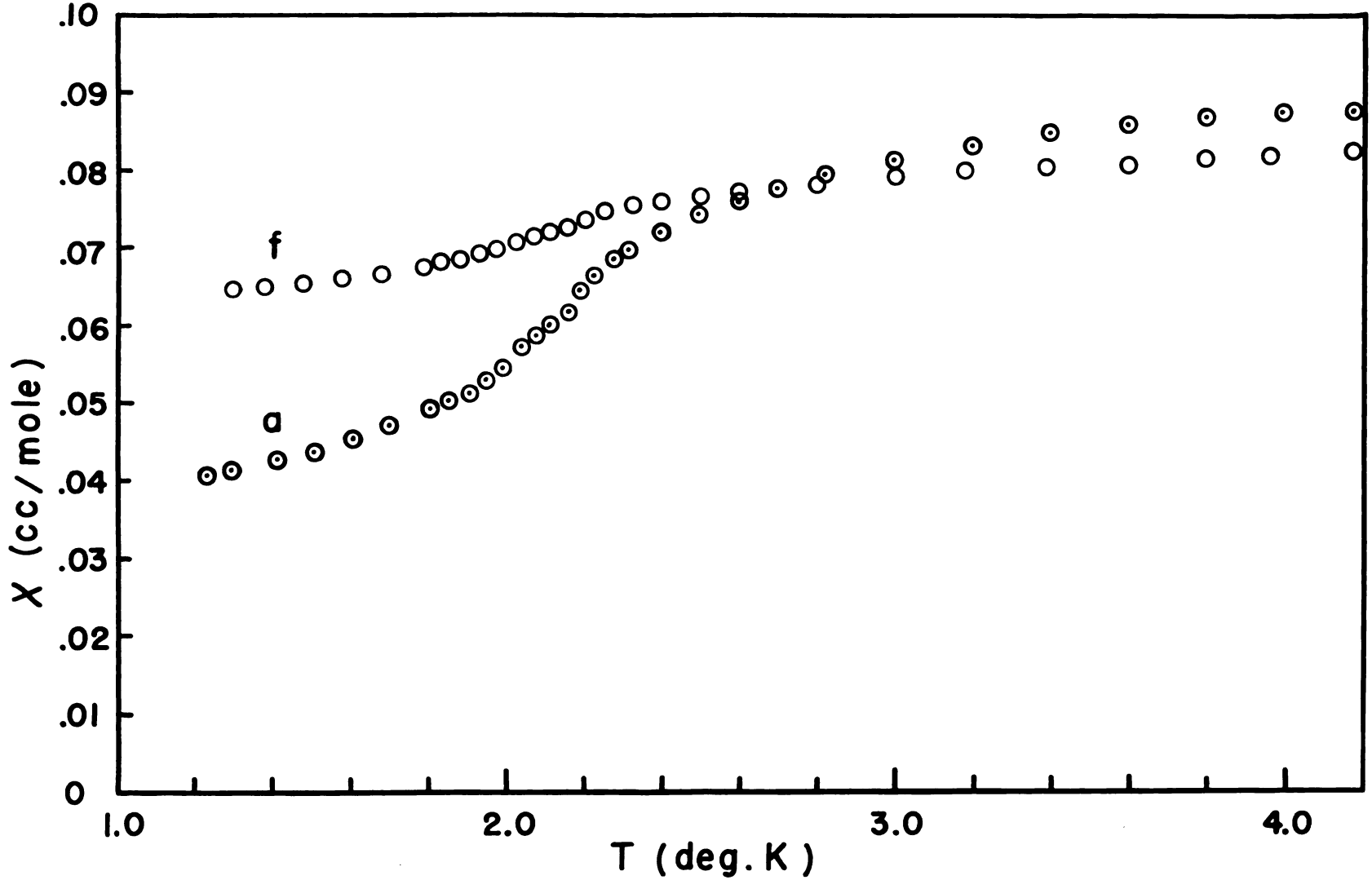

Fig. 27. Magnetic susceptibility of $Ni(tu)_6Br_2$ vs. temperature along the a and f directions.

χ_a vs. T will reveal the presence of inflection points at T = 2.0°K and T = 2.2°K respectively. One should also note at this point that along none of the directions investigated does the magnetic susceptibility approach zero as T → 0°K.

The behavior of the susceptibility in the ac plane is seen more clearly in Fig. 28 which shows the experimental values of χ along the f, a', a, and c directions at T = 1.3°K, and a cosine curve fitted to these values. The directions of the magnetic principal axes in the ac plane are labelled x and z respectively in this drawing. By extrapolation it is estimated that at T = 0°K we would have the following values for the susceptibility along the principal magnetic axes:

$$\chi_x = \chi_{26°} = 0.0310 \text{ cc/mole}$$
$$\chi_y = \chi_b = 0.0920 \text{ cc/mole}$$
$$\chi_z = \chi_{-64°} = 0.0755 \text{ cc/mole}$$

In Tables 9-12 there are listed values of χ and $\chi' = (1 \pm 0.02)\ \chi$ for the susceptibility in the ac plane. The corrected values χ' are used for the following reason: The x and z axes are the principal magnetic axes above and below the transition temperatures. At 4.2°K $\chi_x > \chi_z$ while at 1.3°K $\chi_x < \chi_z$. If these axes remain principal axes at all temperatures between these points, then at some temperature $\chi_x = \chi_z$ and χ is isotropic in the ac plane.

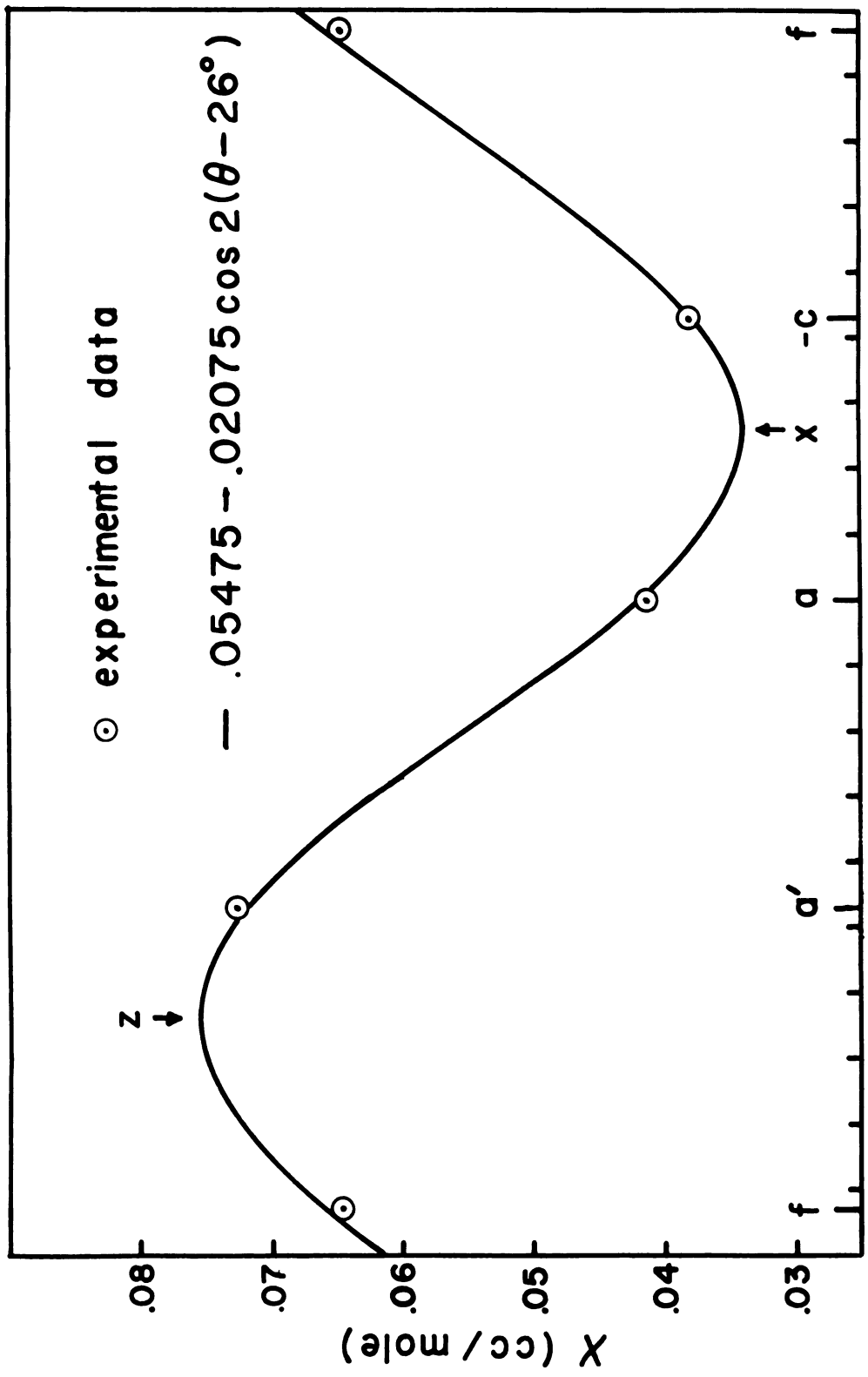

Fig. 28. Magnetic susceptibility of $Ni(tu)_6Br_2$ at 1.3°K as a function of direction in the a c plane.

The 2% corrections listed are such as to allow $\chi_f' = \chi_{a'}' = \chi_a' = \chi_c' = 0.0775$ cc/mole at T = 2.7°K. It is felt that this correction provides more consistent values for the susceptibility in the ac plane.

Figure 29 shows the experimental data listed in Table 16 for the susceptibility of a powdered sample and compares this data with a curve which represents $\frac{1}{3}(\chi_{a'} + \chi_b + \chi_c)$. The a' and c axes are not principal magnetic axes but are reasonably close.

3. Discussion of Sublattice Structure

It has already been noted that the susceptibility along each of the principle magnetic axes approaches a non-zero value as T → 0°K. Thus, a simple two-sublattice model can be eliminated immediately. The next model to be considered is a four-sublattice model in which pairs of antiparallel sublattices lie along different directions and the total magnetization still vanishes. The latter restriction is imposed because none of the susceptibility data indicates a spontaneous net magnetization, which is usually characterized by large values of the susceptibility with a sharp peak at the transition temperature. Unless prohibited by the symmetry properties of the lattice, these sublattice magnetization vectors could lie in any one of the three planes determined by the principal magnetic axes. This implies that alone one of these axes only $\chi_\perp$ will be observed while along the other two both $\chi_\perp$ and $\chi_{\parallel}$ will contribute to the observed susceptibility. The most likely candidate for the perpendicular

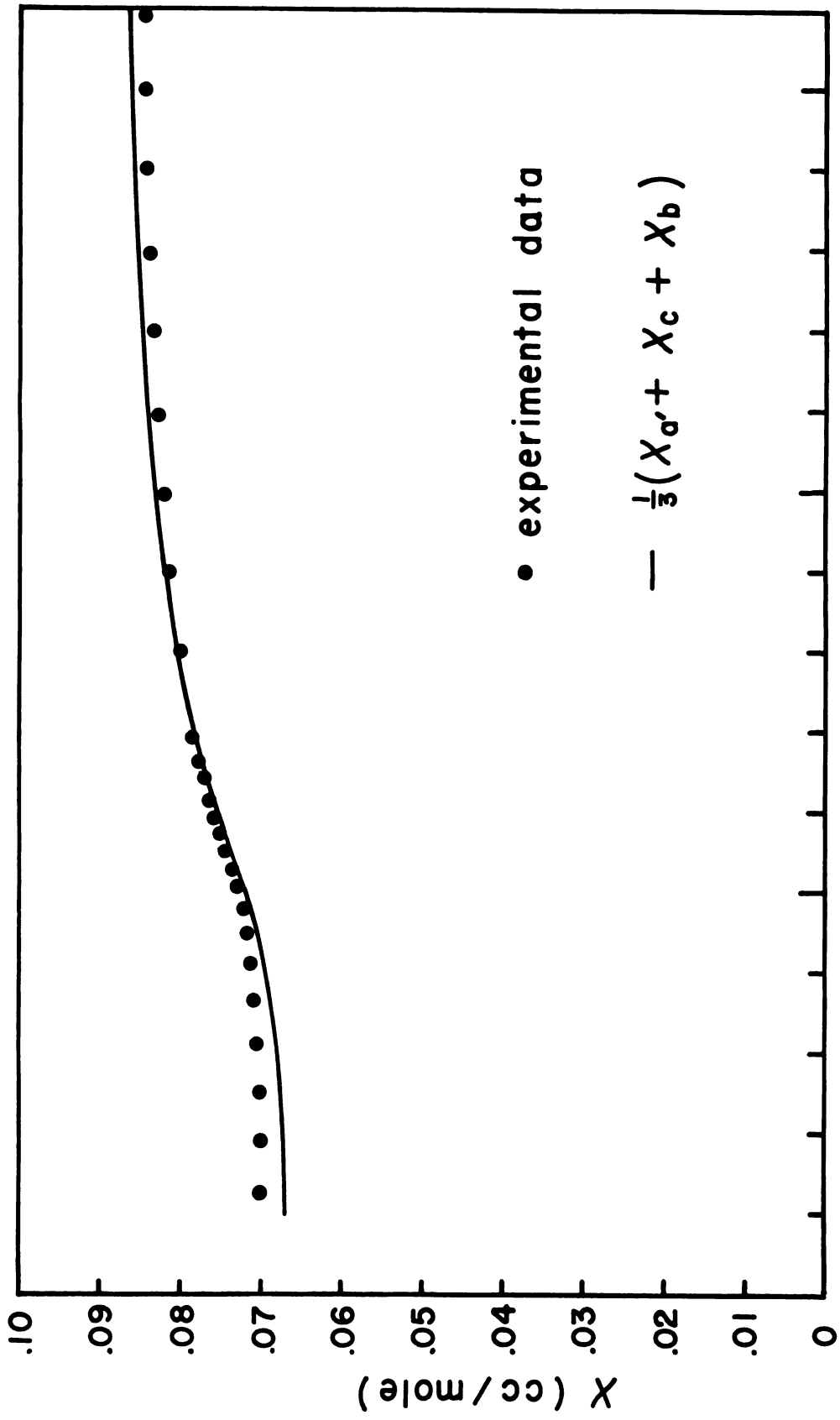

Fig. 29. Magnetic susceptibility of powdered $Ni(tu)_6Br_2$.

direction is the b axis since its low temperature susceptibility is significantly higher than long either of the other two principal axes.

Thus we are led to propose a four sublattice model consisting of two pairs of sublattice magnetization vectors lying in the ac plane. Figure 30 shows the directions of the sublattice magnetization vectors based on this simple model. All vectors lie in the ac plane and make an angle of approximately 33° with the principal axis labelled x.

This sublattice arrangement is based on the following elementary considerations. Assume that the sublattice magnetization vectors lie in the xz (ac) plane. This is the most reasonable choice since χ_y has the largest value at T = 0°K. Let the magnetization vectors make an angle Ø with the axis as shown in Fig. 31. Let the measuring field be represented by $\vec{h}$, making an angle θ with the x axis. If $\chi_{\parallel}$ and $\chi_{\perp}$ are the parallel and perpendicular susceptibilities for either pair of opposing sublattices 1 and 3, or 2 and 4, then in the xz plane the susceptibility is

$$\chi(\theta) = \chi_{\parallel}\cos^2(\theta-\emptyset) + \chi_{\perp}\sin^2(\theta-\emptyset) + \chi_{\parallel}\cos^2(\theta+\emptyset) + \chi_{\perp}\sin^2(\theta+\emptyset) \quad , \tag{4.1}$$

which reduces to

$$\chi(\theta) = (\chi_{\parallel} + \chi_{\perp}) + (\chi_{\parallel} - \chi_{\perp})\cos 2\emptyset \cos 2\theta \quad . \tag{4.2}$$

At T = 0°K , $\chi_{\parallel} = 0$ and $\chi(\theta)$ becomes

$$\chi(\theta) = \chi_{\perp}(1 - \cos 2\emptyset \cos 2\theta) \quad . \tag{4.3}$$

Thus:

$$\left.\begin{aligned} \chi_x &= \chi(0) = \chi_{\perp}(1 - \cos 2\emptyset) = 0.0310 \ , \\ \chi_z &= \chi(\tfrac{\pi}{2}) = \chi_{\perp}(1 + \cos 2\emptyset) = 0.0755 \ . \end{aligned}\right\} \tag{4.4}$$

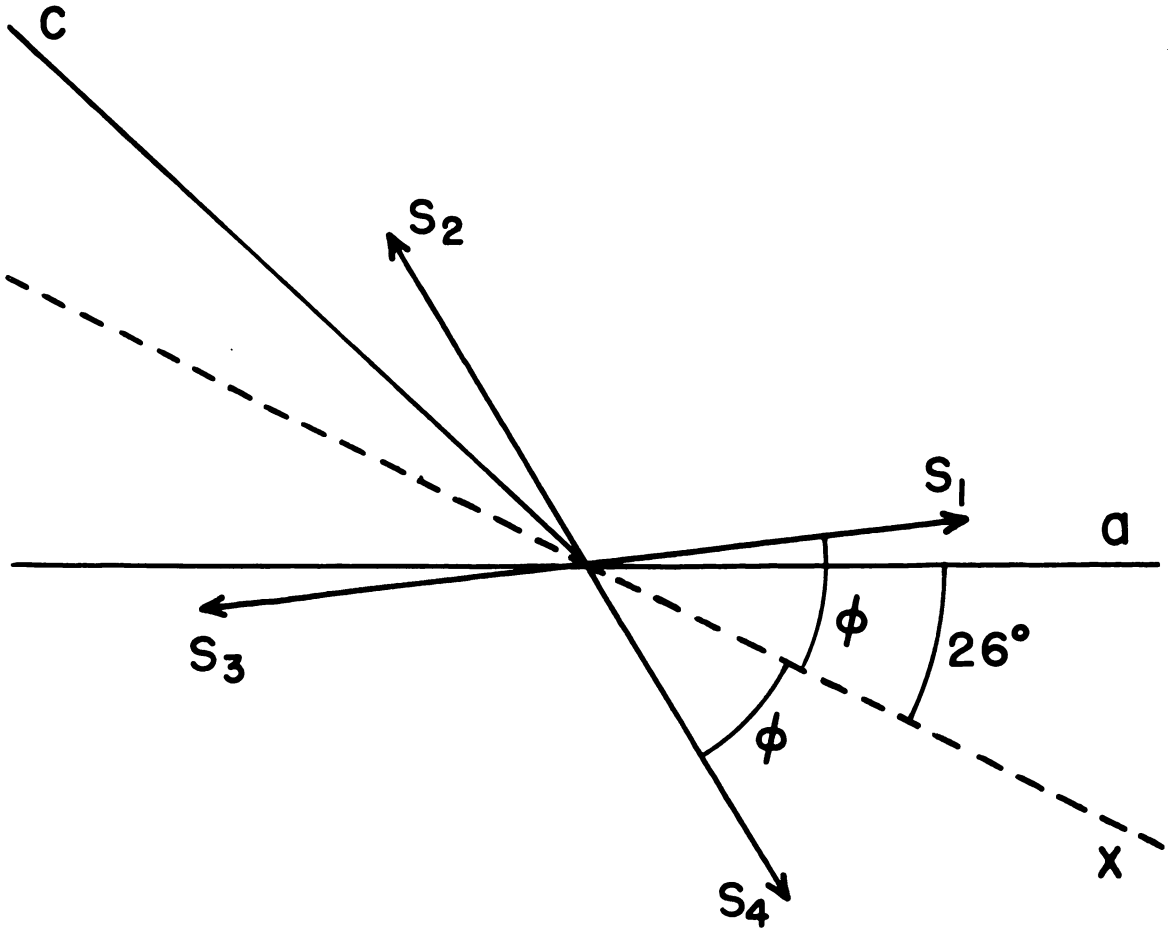

Fig. 30. Possible directions of sublattice magnetization in the ac plane of $Ni(tu)_6Br_2$. ϕ is estimated to be 33°.

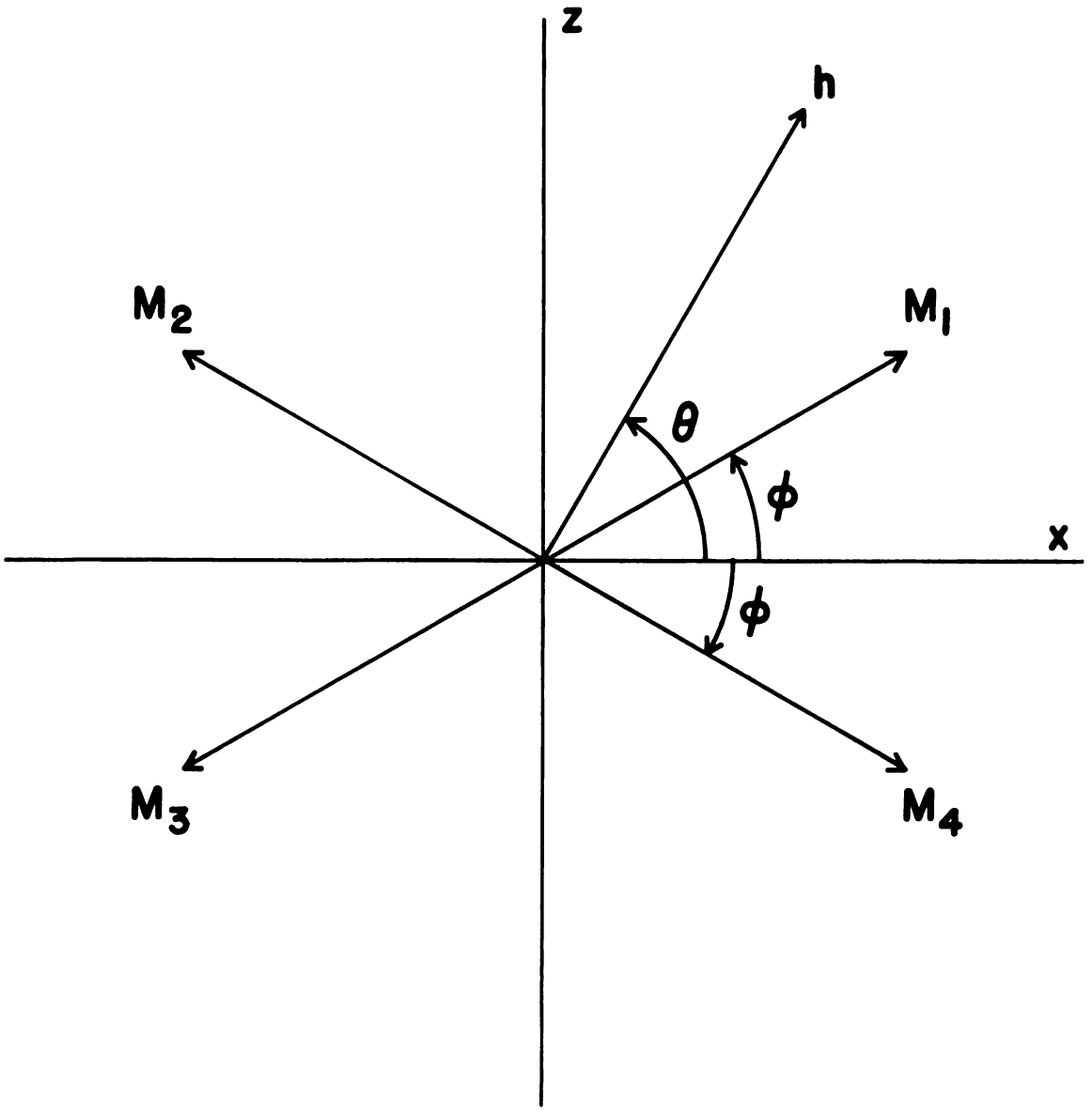

Fig. 31 . Four-sublattice model for susceptibility calculations.

Solving these equations for $\chi_\perp$ and ϕ we get

$$\left.\begin{aligned} 2\chi_\perp &= 0.1065 \quad , \\ \phi &= 33^\circ \quad . \end{aligned}\right\} \qquad (4.5)$$

The value $2\chi_\perp = 0.1065$ compares reasonably well with $\chi_b = 0.0920$ although there is no exact agreement. Crystalline anisotropy could certainly account for such a difference.

The sublattice model here presented is only a suggested model based on susceptibility data alone and should be subjected to further tests such as proton magnetic resonance or neutron diffraction correlated with a detailed crystal structure determination.

4. Discussion of Transition Temperatures

As stated earlier, the magnetic susceptibility along the a and c axes exhibits inflection points at 2.0°K and 2.2°K respectively. This behavior is more clearly seen if $\chi(T)$ is differentiated. As Fisher has shown,[19] the quantity of most interest is the temperature derivative of the product $(\chi_\parallel T)$. This quantity has been calculated from χ_a and χ_c by assuming that $\chi_\perp$ remains constant with temperature and subtracting its contribution in accordance with the proposed sublattice model. This yields:

$$\left.\begin{aligned} 1.25\ \chi_\parallel &= \chi_a - 0.039 \quad , \\ 1.34\ \chi_\parallel &= \chi_c - 0.035 \quad . \end{aligned}\right\} \qquad (4.6)$$

Note that $\chi_{\parallel}$ still applies to only one pair of sublattices, or half of the nickel ions. Figure 32 shows graphically the behavior of $\frac{d(\chi_{\parallel} T)}{dT}$ as a function of the temperature. The peaks in this curve correspond to magnetic transitions of the antiferromagnetic type. Since this derivative is directly proportional to the magnetic contribution to the specific heat it is quite appropriate to compare Fig. 32 to Fig. 33 which shows the specific heat data taken by Forstat, Love, and McElearney. Because of the presence of two peaks in both the susceptibility data and the specific heat data it is concluded that there are indeed two transitions, both magnetic in character. The entropy change calculated by Dr. Forstat from the magnetic contribution to the specific heat is R ln 3, which is consistent with S = 1 for nickel and all spins ordered at T = 0°K.

Possible explanations of the presence of two transitions are that there are two spin systems which order at different temperatures or that there are two types of ordered states which are stable in different temperature ranges. However, without a detailed knowledge of the crystal structure or the spin arrangement it is impossible at this time to make any definite statements concerning these transitions except that they are of the antiferromagnetic type. X ray diffraction and proton magnetic resonance experiments are being carried out by Dr. Spence and his group and should shed considerable light on this problem.

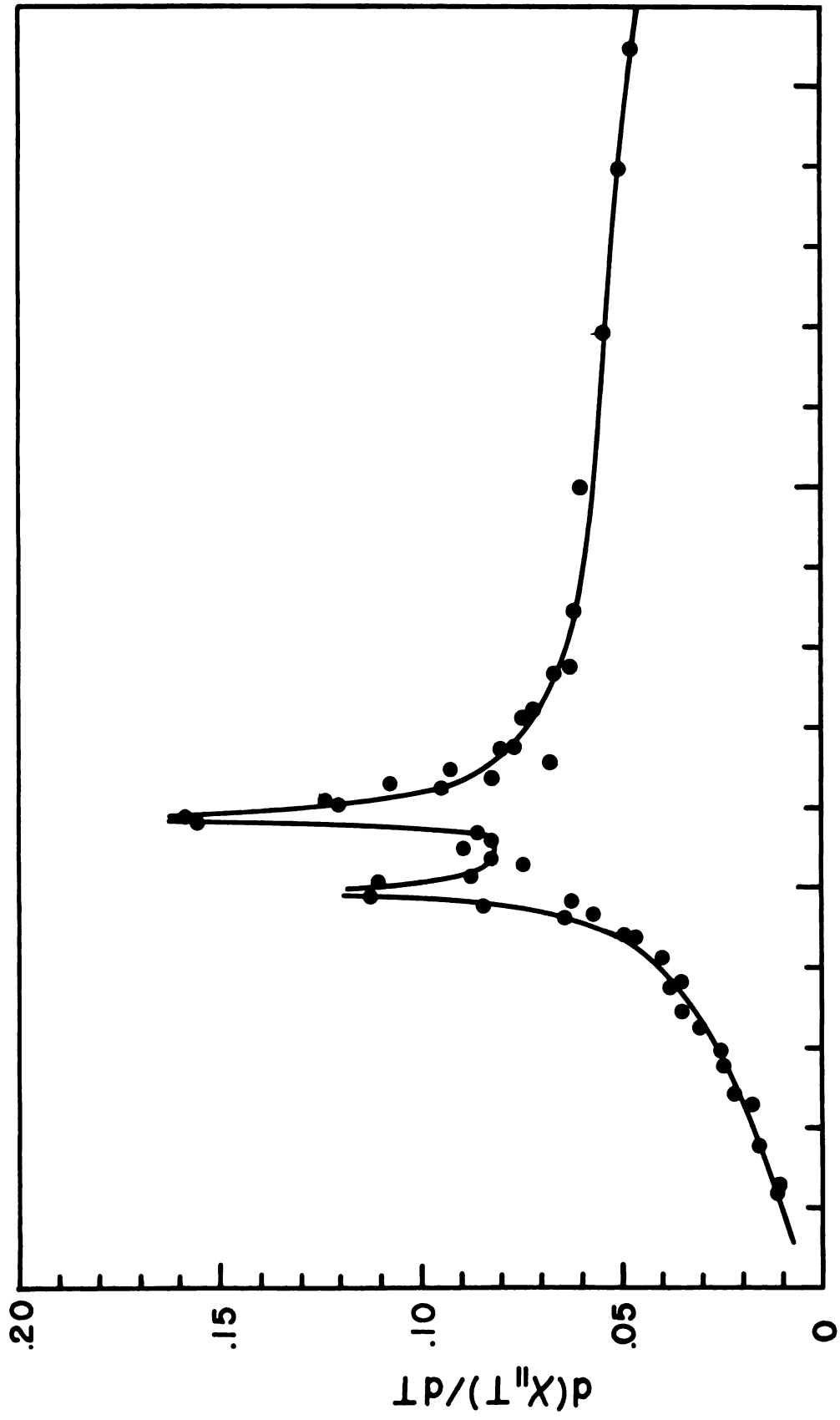

Fig. 32. Plot of $d(\chi_{||}T)/dT$ vs. temperature for $Ni(tu)_6Br_2$.

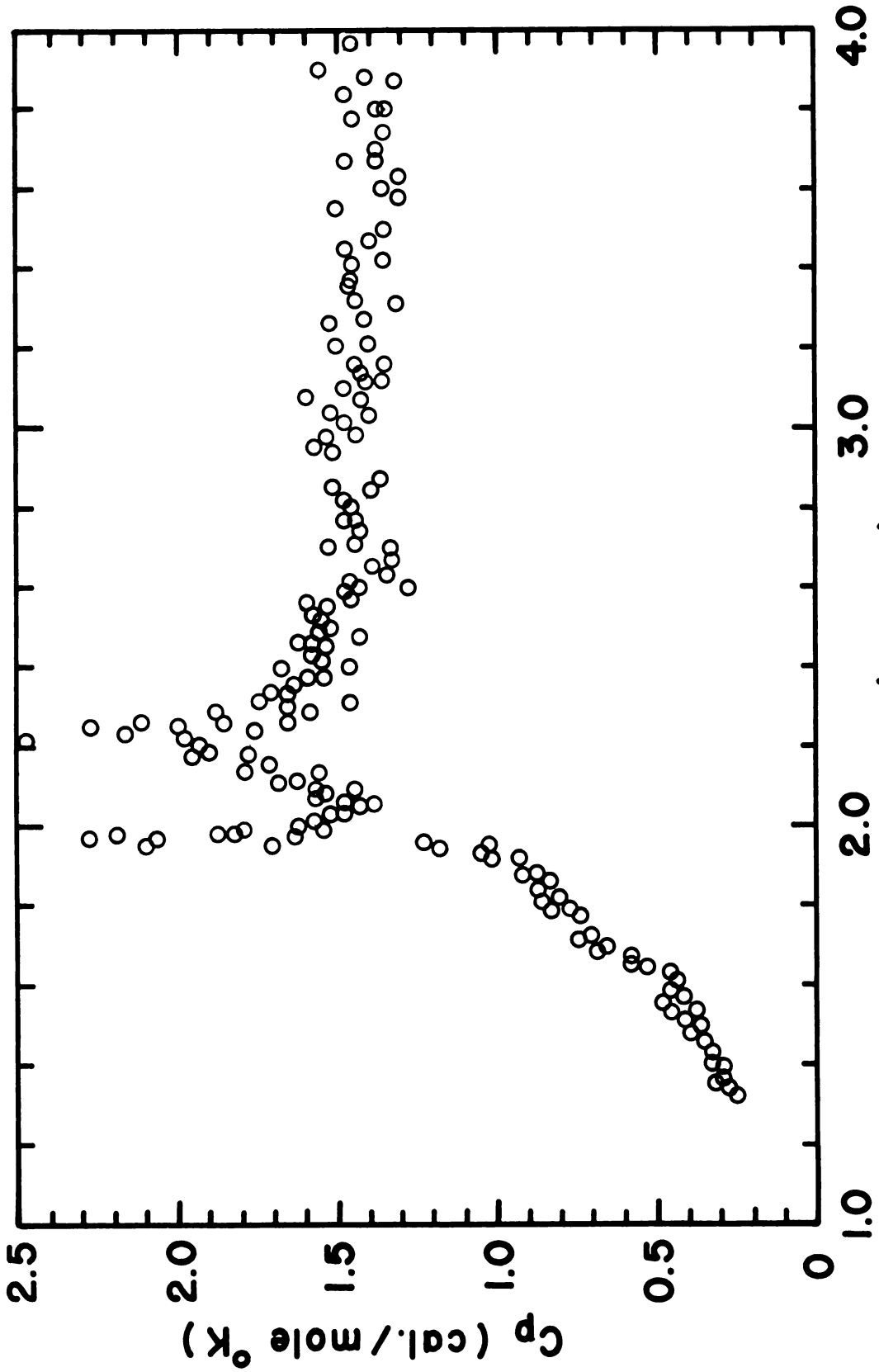

Fig. 33. Molar heat capacity of $Ni(tu)_6Br_2$.

D. Others

In addition to the three materials already discussed, some of the other members of this series of materials were briefly investigated, or should be.

1. $Ni(tu)_4Cl_2$: Hare and Ballhausen[20] have reported that the magnetic susceptibility of this material obeys the relation $\chi = 1.14/(T + 6^\circ)$ in the temperature range from 77°K to 370°K. It was because of this information that the low-temperature properties of this series of compounds was investigated. The proton resonance of $Ni(tu)_4Cl_2$ was observed down to 0.40°K. The resonance lines attained a splitting of about 100 gauss but showed no indication of an antiferromagnetic transition. Low-temperature susceptibility measurements should yet be made on this material.

2. $Fe(tu)_4Cl_2$: The proton resonance investigation of this material gave no evidence for a magnetic transition above 0.40°K. The resonance lines showed a small and rather constant splitting. No susceptibility measurements have yet been made.

3. $Co(tu)_4Br_2$: No magnetic transition above 0.40°K was indicated by proton resonance. This material has not yet been subjected to magnetic susceptibility measurements.

4. $Fe(tu)_6Br_2$: Magnetic susceptibility measurements on a powdered sample indicates an anomaly near 1.0°K which should be investigated further.

5. An unsuccessful attempt was made to grow a thiourea-coordinated manganous bromide. Perhaps this could be pursued further.

6. In addition to the chlorides and bromides considered, the iodides are also worthy of investigation. In particular, $Ni(tu)_6I_2$ grows crystals similar in appearance to $Ni(tu)_6Br_2$.

V. CONCLUSION

The experimental results discussed in Chapter IV indicate that this work has met the objectives set forth in Chapter I. With the apparatus constructed as described in Chapter II the magnetic susceptibility of three new antiferromagnetic materials was measured. Each of these materials is now the subject of further study for the purpose of providing a more complete description of its antiferromagnetic state, which will add to the body of knowledge concerning antiferromagnetic materials upon which a more satisfactory theory of antiferromagnetism can be based.

One unique feature of these materials is the abundance of protons. This makes the analysis of proton resonance data much more difficult than for hydrated materials but allows a more complete mapping of the internal magnetic fields, which may be useful in estimating the distribution of magnetic moment within the crystal giving valuable information concerning the wave functions of the magnetic electrons.

It is of some interest to compare the transition temperatures of the thiourea-coordinated materials with those of the corresponding water-coordinated compounds. Table 2

lists the transition temperatures of the hydrated materials and the thiourea-coordinated materials, along with their ratios.

Table 2.--Comparison of the transition temperatures of the thiourea- and water-coordinated compounds.

Compound	T_N(°K)	Compound	T_N(°K)	Ratio
$CoCl_2 \cdot 6H_2O$	2.28	$Co(tu)_4Cl_2$	0.93	2.45
$MnCl_2 \cdot 4H_2O$	1.68	$Mn(tu)_4Cl_2$	0.56	3.0
$NiBr_2 \cdot 6H_2O$	6.5	$Ni(tu)_6Br_2$	2.2	2.9
$NiCl_2 \cdot 6H_2O$	6.2	$Ni(tu)_4Cl_2$	< 0.4	> 15.5
$FeCl_2 \cdot 4H_2O$	1.0	$Fe(tu)_4Cl_2$	< 0.4	> 2.5
$CoBr_2 \cdot 6H_2O$	3.08	$Co(tu)_4Br_2$	< 0.4	> 7.7

For the three compounds studied in detail the ratio of the transition temperature of the hydrated to the thiourea-coordinated materials is quite uniform. Thus for each pair of materials the ratio of exchange parameters must also be approximately the same. This might also be true for the ferrous chloride type materials. However, for the nickel chloride and cobalt bromide compounds this similarity breaks down. For $Ni(tu)_4Cl_2$ the difference probably results from the fact that its crystal structure is different from $Co(tu)_4Cl_2$ and $Mn(tu)_4Cl_2$. The space group of $Ni(tu)_4Cl_2$ is I4 while the space group of the others is $P4_2/n$.

Structural differences will also most likely account for the fact that $Co(tu)_4Br_2$ behaves differently than $Ni(tu)_6Br_2$. No further statements should be made until the crystal structure analysis of these materials is completed.

REFERENCES

REFERENCES

1. L. Neel, Ann. phys. 17, 64 (1932).

2. H. B. G. Casimir, W. J. de Haas, and D. de Klerk, Physica 6, 241 (1939).

3. W. J. de Haas, and C. J. Gorter, Proc. K. Akad. Amsterdam 7, 676 (1930).

4. W. R. Abel, A. C. Anderson, and J. C. Wheatley, Rev. Sci. Instr. 35, 444 (1964).

5. W. L. Pillinger, P. S. Jastrum, and J. G. Daunt, Rev. Sci. Instr. 29, 159 (1958).

6. T. Nagamiya, K. Yosida, and R. Kubo, Advances in Physics 4, 1 (1955).

7. A. B. Lidiard, Reports on Progress in Physics 17, 201 (1954).

8. C. Domb, Advances in Physics 9, 149, 245 (1960).

9. P. W. Anderson, Phys. Rev. 79, 350 (1950).

10. J. H. Van Vleck, Jour. de Phys. et le Radium 12, 262 (1951).

11. P. W. Anderson, "Exchange in Insulators" in Magnetism edited by George T. Rado and Harry Suhl (Academic Press Inc., New York, 1963) Vol. 1, pp. 25-83.

12. Junjiro Kanamori, "Anisotropy and Magnetostriction of Ferromagnetic and Antiferromagnetic Materials" in Magnetism edited by George T. Rado and Harry Suhl (Academic Press Inc., New York, 1963), Vol. 1, pp. 127-203.

13. L. F. Bates, Modern Magnetism, (Cambridge University Press, 1961) 4th ed., p. 43.

14. T. Oguchi, J. Phys. Soc. Japan 6, 27 (1951).

15. M. F. Sykes and Michael E. Fisher, Physica 28, 919 (1962).

16. Michael E. Fisher and M. F. Sykes, Physica 28, 939 (1962).

17. T. Oguchi, J. Phys. Soc. Japan 6, 31 (1951).

18. M. F. Sykes, J. Math. Phys. 2, 52 (1961).

19. Michael E. Fisher, Phil. Mag. 7, 1731 (1962).

20. C. R. Hare and C. J. Ballhausen, J. Chem. Phys. 40, 788 (1964).

APPENDICES

APPENDIX A

SERIES EXPANSIONS FOR THE PARALLEL SUSCEPTIBILITY OF SOME ANTIFERROMAGNETIC ISING LATTICES

1. Two-dimensional honeycomb lattice

a. $T < T_c = 1.5186519 \frac{|J|}{k}$

From Eq. (8.7), Ref. 15:

$$\chi(T) = \frac{Nm^2}{kT} \left\{ 4y^3 + 12y^5 + 8y^6 + 48y^7 + 96y^8 + 320y^9 + 888y^{10} + 2748y^{11} + 8384y^{12} + 26340y^{13} + 0.1213 \sum_{n=12}^{\infty} \frac{(y/y_c)^{n+2}}{n(n+1)} \right\}$$

Where: $y = \exp(-2|J|/kT)$

$y_c = 0.2679492$

b. $T > T_c = 1.5186519 \frac{|J|}{k}$

From Eqs. (7.6) and (7.7), Ref. 15:

$$\chi(T) = \frac{Nm^2}{kT} \left\{ (1-\sqrt{3}\,v)^{-\frac{7}{4}} (1+3v^2)^{-\frac{1}{8}} \exp \left[\sum_{n=1}^{24} f_n t^n + R_{24}(t) \right] \right\}$$

$$R_{24}(t) = -[0.184t + 0.42t^2 + 0.150t^3 - 0.07t^4] \sum_{r=6}^{\infty} \frac{t^{4r}}{r(r+1)}$$

Where: $v = \tanh(J/kT)$

$t = v/v_c$

$v_c = -0.5773503$

and the f_n are given by:

$f_1 = +0.017949$	$f_9 = -0.040772$	$f_{17} = -0.009535$
$f_2 = -0.250000$	$f_{10} = -0.050000$	$f_{18} = -0.019243$
$f_3 = +0.005983$	$f_{11} = -0.012624$	$f_{19} = -0.007160$
$f_4 = -0.083333$	$f_{12} = +0.005144$	$f_{20} = +0.002436$
$f_5 = -0.073390$	$f_{13} = -0.017627$	$f_{21} = -0.006252$
$f_6 = -0.083333$	$f_{14} = -0.030227$	$f_{22} = -0.013244$
$f_7 = -0.015764$	$f_{15} = -0.010208$	$f_{23} = -0.004891$
$f_8 = -0.004630$	$f_{16} = +0.003629$	$f_{24} = +0.001889$

2. Two-Dimensional Plane Square Lattice

a. $T < T_c = 2.2621852 \frac{|J|}{k}$

From Eq. (6.7), Ref. 15:

$$\chi(T) = \frac{Nm^2}{kT} \left\{ 4y^4 + 16y^8 + 32y^{10} + 156y^{12} + 608y^{14} + 0.084 \sum_{n=6}^{\infty} \frac{(y/y_c)^{2n+2}}{n(n+1)} \right\}$$

where: $y = \exp(-2|J|/kT)$

$y_c = 0.4142136$

b. $T > T_c = 2.2621852 \frac{|J|}{k}$

Eq. (5.18), Ref. 15, should be corrected to read:

$$\chi(T) = \frac{Nm^2}{kT} \left\{ (1-2v-v^2)^{-\frac{7}{4}} \exp \left[\sum_{n=1}^{16} d_n t^n - 2.022 \sum_{n=17}^{\infty} \frac{(-t)^n}{n(n+1)} \right] \right\}$$

where: $v = \tanh(J/kT)$

$t = v/|v_c|$

$v_c = -0.4142136$

and the d_n are given by:

$d_1 = +0.20711$ $\quad$ $d_9 = +0.02203$

$d_2 = -0.21447$ $\quad$ $d_{10} = -0.01788$

$d_3 = +0.08291$ $\quad$ $d_{11} = +0.01484$

$d_4 = -0.08463$ $\quad$ $d_{12} = -0.01268$

$d_5 = +0.04999$ $\quad$ $d_{13} = +0.01095$

$d_6 = -0.04251$ $\quad$ $d_{14} = -0.00959$

$d_7 = +0.03571$ $\quad$ $d_{15} = +0.00840$

$d_8 = -0.02811$ $\quad$ $d_{16} = -0.00743$

3. Three-Dimensional Simple Cubic Lattice

a. $T < T_c = 4.51032 \dfrac{|J|}{k}$

From Eqs. (4.3) and (4.4), Ref. 16:

$$\chi(T) = \frac{Nm^2}{kT} \left\{ 4y^6 - 8y^{12} + 37.724y^{14}/(1 + 3.23y^2) + 22.28y^{14} - 22.15y^{16} + 22.43y^{18} + 23.23y^{20} + 93.92y^{22} - 14.64y^{24} + 98.00y^{26} + 295.88y^{28} + 0.329 \sum_{n=15}^{\infty} \frac{(y/y_c)^{2n}}{n(n+1)} \right\}$$

where: $y = \exp(-2|J|/kT)$

$y_c = 0.64183$

b. $T > T_c = 4.51032 \dfrac{|J|}{k}$

Eq. (3.9), Ref. 16, must be corrected to read:

$$\chi(T) = \frac{Nm^2}{kT} \left\{ (1 + t)^{-\frac{5}{4}} \exp \left[- \sum_{n=1}^{11} f_n t^n - R_{11}(t) \right] \right\}$$

where: $v = \tanh (J/kT)$

$t = v/v_c$

$v_c = -0.21815$

Eq. (3.7) must be corrected to read:

$$R_{11}(t) = 0.338 \left[1 + \frac{(1-t)}{t} \ln(1-t) - \sum_{n=1}^{11} \frac{t^n}{n(n+1)} \right]$$

and the f_n are given by:

$f_1 = 0.058901$ $\quad$ $f_7 = 0.0059701$

$f_2 = 0.053926$ $\quad$ $f_8 = 0.0046536$

$f_3 = 0.019362$ $\quad$ $f_9 = 0.0037844$

$f_4 = 0.013552$ $\quad$ $f_{10} = 0.0030197$

$f_5 = 0.011461$ $\quad$ $f_{11} = 0.0026244$

$f_6 = 0.0078652$

4. Three-Dimensional Body-Centered Cubic Lattice

a. $T < T_c = 6.35080 \frac{|J|}{k}$

From Eq. (4.7), Ref. 16:

$$\chi(T) = \frac{Nm^2}{kT} \left\{ 4y^8 - 8y^{16} + 112y^{20} - 256y^{22} + 96y^{24} + R_{24}(y) \right\}$$

Eq. (4.8) must be corrected to read:

$$R_{24}(y) = 1.22 \sum_{n=13}^{\infty} \frac{(y/y_c)^{2n}}{n(n+1)}$$

where: $y = \exp(-2|J|/kT)$

$y_c = 0.72985$

b. $T > T_c = 6.35080 \frac{|J|}{k}$

Eq. (3.9), Ref. 16 must be corrected to read:

$$\chi(T) = \frac{Nm^2}{kT} (1+t)^{\frac{5}{7}} \exp \left[- \sum_{n=1}^{9} f_n t^n - R_9(t) \right]$$

Eq. (3.7), Ref. 16 must be corrected to read:

$$R_9(t) = 0.30 \left[1 + \frac{(1-t)}{t} \ln(1-t) - \sum_{n=1}^{9} \frac{t^n}{n(n+1)} \right]$$

where: $t = v/v_c$

$v = \tanh (J/kT)$

$v_c = -0.15617$

and the f_n are given by:

$f_1 = -0.000625$

$f_2 = +0.039648$

$f_3 = +0.020097$

$f_4 = +0.012693$

$f_5 = +0.008782$

$f_6 = +0.006726$

$f_7 = +0.005124$

$f_8 = +0.003954$

$f_9 = +0.003400$

Table 3.--Parallel susceptibility for honeycomb, plane square, simple cubic, and body-centered cubic lattices as computed from the Ising model series expansions.

T/T_c	χ/χ_c			
	Honeycomb	Plane Square	Simple Cubic	Body-centered Cubic
.00	.000	.000	.000	.000
.05	.000	.000	.000	.000
.10	.000	.000	.000	.000
.15	.000	.000	.000	.000
.20	.000	.000	.000	.000
.25	.000	.000	.001	.002
.30	.000	.001	.005	.008
.35	.001	.003	.017	.023
.40	.004	.009	.038	.050
.45	.011	.022	.071	.088
.50	.025	.043	.116	.139
.55	.046	.076	.170	.200
.60	.079	.119	.232	.268
.65	.123	.174	.304	.340
.70	.182	.240	.382	.413
.75	.255	.321	.463	.489
.80	.343	.410	.551	.564
.85	.450	.516	.643	.642
.90	.581	.636	.740	.723
.95	.741	.782	.850	.819
1.00	1.000	.1000	1.000	1.000
1.05	1.256	1.201	1.024	1.017
1.10	1.382	1.314	1.028	1.015
1.15	1.485	1.390	1.025	1.009
1.20	1.556	1.441	1.019	1.000

Table 3.--Continued.

T/T_c	x/x_c			
	Honeycomb	Plane Square	Simple Cubic	Body-centered Cubic
1.3	1.643	1.507	1.001	.976
1.4	1.697	1.539	.980	.950
1.5	1.726	1.550	.956	.926
1.6	1.740	1.550	.932	.898
1.7	1.742	1.540	.908	.873
1.8	1.738	1.526	.886	.848
1.9	1.728	1.509	.863	.826
2.0	1.716	1.488	.842	.802
2.1	1.698	1.467	.819	.781
2.2	1.681	1.444	.799	.761
2.3	1.660	1.420	.781	.740
2.4	1.640	1.397	.761	.721
2.5	1.619	1.373	.744	.704
2.6	1.596	1.350	.726	.687
2.7	1.575	1.327	.710	.669
2.8	1.552	1.303	.693	.654
2.9	1.531	1.282	.679	.638
3.0	1.507	1.260	.664	.625
3.1	1.486	1.238	.649	.611
3.2	1.463	1.217	.636	.599
3.3	1.443	1.196	.623	.585
3.4	1.423	1.176	.611	.573
3.5	1.400	1.156	.599	.563
3.6	1.382	1.137	.587	.551
3.7	1.362	1.118	.576	.540
3.8	1.341	1.101	.564	.530
3.9	1.323	1.084	.555	.520

Table 3.--Continued

T/T_c	x/x_c			
	Honeycomb	Plane Square	Simple Cubic	Body-Centered Cubic
4.0	1.304	1.068	.544	.510
4.2	1.267	1.035	.526	.492
4.4	1.233	1.004	.507	.475
4.6	1.201	.975	.491	.460
4.8	1.169	.946	.475	.444
5.0	1.138	.919	.461	.430

APPENDIX B

SUSCEPTIBILITY DATA IN TABULAR FORM

Table 4.--Magnetic susceptibility data for $Co(tu)_4Cl_2$ along the [001] axis in units of cc/mole.

T°K	χ_{001}	T°K	χ_{001}
0.459	.0630	1.212	.566
.478	.0661	1.318	.574
.512	.0676	1.393	.577
.547	.0718	1.495	.579
.581	.0850	1.604	.579
.613	.101	1.732	.575
.638	.115	1.814	.571
.666	.135	1.899	.567
.700	.162	1.999	.562
.727	.185	2.120	.555
.750	.208	2.220	.547
.776	.236	2.290	.544
.800	.263	2.410	.532
.830	.296	2.470	.530
.843	.331	2.602	.519
.861	.354	2.786	.505
.875	.376	3.000	.487
.895	.412	3.194	.472
.915	.432	3.406	.459
.942	.495	3.595	.446
.979	.421	3.786	.436
1.050	.543	3.998	.425
1.120	.555	4.194	.418

Table 5.--Magnetic susceptibility data for $Co(tu)_4Cl_2$ along the [110] axis in units of cc/mole.

T°K	χ_{110}	T°K	χ_{110}
.455	.222	1.694	.377
.500	.224	1.814	.369
.549	.225	1.938	.360
.595	.229	2.083	.348
.653	.236	2.107	.348
.700	.245	2.195	.342
.750	.257	2.326	.333
.800	.272	2.470	.322
.842	.292	2.602	.314
.888	.317	2.782	.304
.919	.338	3.004	.292
.955	.366	3.221	.283
1.007	.381	3.411	.275
1.194	.394	3.608	.270
1.292	.391	3.802	.264
1.391	.388	4.012	.257
1.560	.382	4.2	.251

Table 6.--Magnetic susceptibility data for Co)tu)$_4$Cl$_2$ along the [100] axis in units of cc/mole.

T°K	χ_{100}	T°K	χ_{100}
0.450	.266	1.571	.423
.515	.267	1.810	.411
.613	.274	2.001	.398
.700	.289	2.197	.384
.750	.302	2.398	.371
.800	.318	2.602	.359
.851	.347	2.800	.348
.880	.361	3.000	.337
.911	.386	3.200	.328
.939	.404	3.396	.319
.970	.414	3.608	.310
1.000	.424	3.802	.303
1.085	.432	4.006	.295
1.201	.433	4.2	.288
1.404	.430		

Table 7.--Magnetic susceptibility data for powdered $Co(tu)_4Cl_2$ in units of cc/mole.

T°K	χ_p	T°K	χ_p
0.452	.172	1.812	.439
.555	.180	2.000	.428
.643	.202	2.200	.414
.720	.228	2.420	.399
.800	.271	2.602	.388
.855	.320	2.800	.376
.904	.366	3.000	.365
.951	.420	3.193	.355
1.007	.435	3.398	.346
1.090	.448	3.610	.337
1.170	.451	3.804	.329
1.318	.455	4.017	.321
1.401	.454	4.185	.314
1.592	.449		

Table 8.--Magnetic susceptibility data for $Mn(tu)_4Cl_2$ along [001] axis in units of cc/mole.

T°K	χ_{001}	T°K	χ_{001}
.422	1.36	1.506	1.14
.472	1.39	1.658	1.09
.513	1.41	1.685	1.08
.543	1.43	1.810	1.03
.573	1.46	1.893	1.008
.621	1.49	2.003	.971
.672	1.48	2.095	.944
.722	1.47	2.290	.885
.770	1.46	2.493	.831
.832	1.44	2.694	.783
.880	1.42	2.900	.737
.938	1.39	3.162	.684
1.014	1.35	3.396	.642
1.107	1.31	3.608	.606
1.182	1.27	3.806	.577
1.327	1.21	4.009	.550
1.352	1.20	4.2	.528
1.480	1.16		

Table 9.--Magnetic susceptibility data for $Mn(tu)_4Cl_2$ along the [100] axis in units of cc/mole.

T°K	χ_{100}	T°K	χ_{100}
.477	1.904	1.663	1.688
.498	1.998	1.715	1.654
.532	2.043	1.770	1.634
.558	2.126	1.858	1.590
.583	2.217	1.873	1.568
.625	2.258	1.986	1.532
.670	2.262	2.012	1.511
.720	2.257	2.090	1.473
.770	2.244	2.090	1.464
.837	2.213	2.216	1.414
.911	2.163	2.309	1.379
.961	2.110	2.371	1.355
1.050	2.042	2.529	1.300
1.072	2.032	2.789	1.220
1.226	1.941	2.989	1.167
1.347	1.861	3.299	1.090
1.453	1.798	3.510	1.045
1.458	1.800	3.665	1.015
1.556	1.744	4.016	.951
1.605	1.714	4.2	.922

Table 10.--Magnetic susceptibility data for $Mn(tu)_4Cl_2$ along the [110] axis in units of cc/mole.

T°K	χ_{110}	T°K	χ_{110}
.433	1.73	1.208	1.85
.472	1.82	1.383	1.75
.512	1.91	1.395	1.74
.519	1.94	1.515	1.67
.533	1.95	1.596	1.63
.552	1.99	1.701	1.56
.560	2.04	1.794	1.53
.565	2.06	1.855	1.48
.581	2.13	2.007	1.43
.606	2.17	2.125	1.38
.637	2.18	2.375	1.27
.656	2.18	2.650	1.18
.703	2.17	2.891	1.11
.746	2.16	3.143	1.04
.777	2.14	3.414	.982
.851	2.11	3.444	.980
.926	2.05	3.633	.937
1.012	2.00	3.904	.880
1.105	1.93	4.20	.835

Table 11.--Magnetic susceptibility of $Ni(tu)_6Br_2$ along the b axis in units of cc/mole.

T°K	$10^4\chi_b$	T°K	$10^4\chi_b$
1.191	910	2.264	857
1.398	904	2.327	859
1.508	897	2.401	863
1.596	893	2.497	867
1.700	885	2.590	872
1.802	881	2.809	885
1.875	877	2.992	896
1.909	875	3.196	907
1.955	873	3.393	916
1.993	870	3.575	923
2.047	866	3.769	932
2.094	864	4.007	940
2.139	863	4.188	943
2.178	857		
2.220	858		

Table 12.--Magnetic susceptibility of $Ni(tu)_6Br_2$ along the a' axis in units of cc/mole. $\chi'_{a'} = 0.98\ \chi_{a'}$.

T°K	$10^4\chi_{a'}$	$10^4\chi'_{a'}$	T°K	$10^4\chi_{a'}$	$10^4\chi'_{a'}$
1.216	742	727	2.278	775	760
1.404	741	726	2.327	778	763
1.504	741	726	2.405	781	765
1.635	743	728	2.590	787	771
1.750	744	729	2.780	791	776
1.837	746	731	2.996	795	779
1.913	748	733	3.190	798	782
1.977	752	737	3.385	799	783
2.036	756	741	3.585	800	784
2.085	759	744	3.791	799	783
2.137	762	747	3.994	798	782
2.181	767	752	4.200	795	779
2.222	771	755			

Table 13.--Magnetic susceptibility of $Ni(tu)_6Br_2$ along the c axis in units of cc/mole. $\chi'_c = 0.98\ \chi_c$.

T°K	$10^4\chi_c$	$10^4\chi'_c$	T°K	$10^4\chi_c$	$10^4\chi'_c$
1.20	376	370	2.226	667	654
1.306	387	379	2.255	687	673
1.427	402	394	2.294	700	686
1.548	422	413	2.332	712	697
1.638	437	428	2.375	725	710
1.726	458	448	2.477	751	736
1.801	474	464	2.602	776	760
1.919	507	497	2.985	831	814
1.966	523	512	3.184	851	834
2.009	551	540	3.398	866	849
2.061	576	565	3.597	879	861
2.102	593	582	3.802	889	871
2.149	613	601	3.988	894	876
2.185	649	636	4.195	900	882

Table 14.--Magnetic susceptibility of $Ni(tu)_6Br_2$ along direction f in units of cc/mole. $\chi'_f = 1.02\chi_f$.

T°K	$10^4\chi_f$	$10^4\chi'_f$	T°K	$10^4\chi_f$	$10^4\chi'_f$
1.299	633	646	2.205	721	736
1.382	637	650	2.254	731	746
1.479	641	654	2.326	737	751
1.582	647	660	2.405	743	758
1.682	654	667	2.503	750	765
1.787	663	676	2.602	755	770
1.831	670	683	2.805	766	781
1.884	672	686	3.003	775	791
1.933	676	690	3.178	781	797
1.983	683	696	3.393	787	802
2.026	691	705	3.590	791	806
2.071	698	712	3.795	796	812
2.114	704	718	3.965	802	818
2.158	709	724	4.191	806	825

Table 15.--Magnetic susceptibility of $Ni(tu)_6Br_2$ along the a axis in units of cc/mole. $\chi'_a = 1.02\ \chi_a$.

T°K	$10^4\chi_a$	$10^4\chi'_a$	T°K	$10^4\chi_a$	$10^4\chi'_a$
1.235	401	409	2.230	651	665
1.296	406	414	2.280	672	685
1.417	418	427	2.313	684	697
1.510	430	438	2.400	706	720
1.606	444	453	2.494	726	741
1.700	461	470	2.601	744	759
1.811	483	493	2.700	760	775
1.854	492	502	2.802	773	788
1.911	505	516	3.000	795	811
1.950	518	529	3.200	815	831
1.994	532	543	3.400	830	847
2.041	560	571	3.604	841	857
2.080	574	585	3.804	850	866
2.115	589	600	4.000	856	873
2.161	606	618	4.20	859	876
2.196	633	646			

Table 16.--Magnetic susceptibility of powdered $Ni(tu)_6Br_2$ in units of cc/mole.

T°K	$10^4 x_p$	T°K	$10^4 x_p$
1.257	700	2.232	762
1.387	701	2.290	771
1.507	701	2.325	774
1.625	704	2.394	783
1.735	708	2.607	800
1.823	711	2.793	813
1.898	715	2.993	821
1.958	721	3.190	829
2.015	729	3.395	835
2.061	735	3.591	839
2.106	741	3.797	843
2.150	747	3.987	844
2.190	757	4.200	844